

A GPU-accelerated Nonlinear Branch-and-Bound Framework for Sparse Linear Models

Xiang Meng

MIT Operations Research Center
`mengx@mit.edu`

Ryan Lucas

MIT Operations Research Center
`ryanlu@mit.edu`

Rahul Mazumder

MIT Sloan School of Management, ORC, and MIT Center for Statistics
`rahulmaz@mit.edu`

Abstract

We study exact sparse linear regression with an ℓ_0 – ℓ_2 penalty and develop a branch-and-bound (BnB) algorithm that is explicitly designed for GPU execution. Starting from a perspective reformulation, we derive an interval relaxation that can be solved by ADMM with closed-form, coordinate-wise updates. We structure these updates so that the main work at each BnB node reduces to batched matrix–vector operations with a shared data matrix, enabling fine-grained parallelism across coordinates and coarse-grained parallelism across many BnB nodes on a single GPU. Feasible solutions (upper bounds) are generated by a projected gradient method on the active support, which is implemented in a batched fashion so that many candidate supports are updated in parallel on the GPU. We discuss practical design choices such as memory layout, batching strategies, and load balancing across nodes that are crucial for obtaining good utilization on modern GPUs. On synthetic and real high-dimensional datasets, our GPU-based approach achieves clear runtime improvements over a CPU implementation of our method, an existing specialized BnB method, and commercial MIP solvers.

Keywords: Branch-and-Bound; Mixed Integer Programming; Sparse Learning; GPU

1 Introduction

Mixed integer programming (MIP) and especially mixed integer nonlinear programming (MINLP), has emerged as a promising tool for modeling and computation of foundational statistics and machine learning (ML) problems that admit a combinatorial description [10]. Common examples include problems such as high dimensional sparse regression [33, 12], graphical models [6], decision trees [9], robust statistics (outlier detection) [28], among others [54]. MIP-based estimators in high-dimensional statistics are known to enjoy optimal statistical properties in suitable regimes [58, 60, 25, 39, 7, 32].

In this paper we focus on a canonical problem from this family, the sparse linear regression with ℓ_2 regularization. Given a dataset $(X, y) \in \mathbb{R}^{n \times p} \times \mathbb{R}^n$, where X is the design matrix containing n samples and p features, and y is the response vector, the problem can be formulated as:

$$\min_{\beta \in \mathbb{R}^p} \frac{1}{2} \|y - X\beta\|_2^2 + \lambda_0 \|\beta\|_0 + \lambda_2 \|\beta\|_2^2, \quad (1)$$

where β denotes the regression coefficients, The ℓ_0 norm $\|\beta\|_0$ counts the number of nonzero elements in β and the squared ℓ_2 -norm $\|\beta\|_2^2$ imposes a penalty on the magnitude of the coefficients. The

regularization parameters $\lambda_0 \geq 0$ and $\lambda_2 \geq 0$ are hyperparameters selected by practitioners to control the trade-off between model fit, sparsity, and shrinkage. Specifically, λ_0 controls the level of sparsity by penalizing the inclusion of less relevant features, while λ_2 regulates the degree of shrinkage applied to the coefficients. Several works have explored the statistical properties of ℓ_0 -based estimators [27, 16, 61, 24, 57, 19]. Under suitable assumptions, global solutions to problem (1) achieve optimal support recovery [20] and prediction error bounds [48]. These strong guarantees generally do not extend to approximate solutions obtained from heuristic methods. Moreover, [40] demonstrates that the ℓ_2 term helps mitigate overfitting in low signal-to-noise ratio (SNR) settings.

Despite its merit, solving problem (1) poses substantial computational challenges as the problem is \mathcal{NP} -hard [42]. Significant efforts have been devoted to developing exact algorithms based on MIP. Off-the-shelf MIP solvers reformulate the problem into a MIP framework and leverage powerful branch-and-bound (BnB) techniques inherent in commercial solvers like Gurobi and CPLEX. These MIP solvers can solve moderate-sized instances of (1), with $n \sim p \lesssim 10^3$, to global optimality, but struggle with larger instances [11]. There have been several works designing specialized algorithms that are capable of handling larger-scale problems within a MIP framework [33, 12, 30, 5]. Nevertheless, often the computational burden of certifying global optimality often requires traversing a massive BnB search tree, which can result in large run-times. We aim to advance the computational practice of solving problem (1) by significantly reducing the time required to certify optimality for large-scale problems. Different from earlier work in this area, we consider algorithmic development keeping in mind hardware-algorithm co-design.

Existing algorithms for problem (1) are designed to run on classical CPU architectures, while approaches designed to be run on more scalable computing hardware such as GPUs have been explored to a lesser extent (see section 1.1). A GPU can perform on the order of tens of trillions of floating point operations per second, where a typical CPU does orders less [51]. GPUs have been used extensively in scientific computing to accelerate compute-intensive workloads in fields such as atmospheric modelling [35] and physical simulations [43], among others. GPU-based computing has also become the central paradigm powering the enormous success of deep learning approaches for high-dimensional unstructured data [41, 15, 46]. More recently, GPUs have also begun to be used in optimization, a notable example being specialized linear programming solvers that exploit parallelism on GPUs [34, 52, 53, 38]. However, their implications beyond this family of problems especially non-linear BnB remain to be fully explored.

The integration of GPUs into a BnB framework is non-trivial due to a fundamental mismatch between the hardware and traditional algorithms. GPUs are designed for massive parallelism, and excel when executing identical operations across large blocks of data, whereas BnB involves traversing a search tree in an irregular manner. To fully leverage GPU acceleration, in this paper we develop new algorithmic methodology integrating different components of a non-linear BnB framework that exploit parallel execution to solve problem (1). For the node relaxation algorithm, we propose an integrated approach centered on a specialized First-Order Method (FoM) designed for simultaneous variable updates at each node. Specifically, the updates within our FoM are parallelizable across the elements of the decision variables, which leads to large speed-ups when executed on GPUs. A direct consequence of this FoM is the ability to compute sparse primal solutions and valid dual bounds. Furthermore, this algorithmic structure allows for the simultaneous solving of multiple subproblems, enabling parallelism *across the BnB nodes*, leading to faster exploration of the tree and consequently faster dual bound certification. Finally, we design the algorithm so that the decision variables can be heavily warm-started, leading to significant reductions in per-node solve times as the tree is traversed. As illustrated in Figure 1, we keep the lightweight BnB logic including node selection, branching, and global bound updates on the CPU, while offloading the computationally expensive lower- and upper-bound algorithms to the GPU.

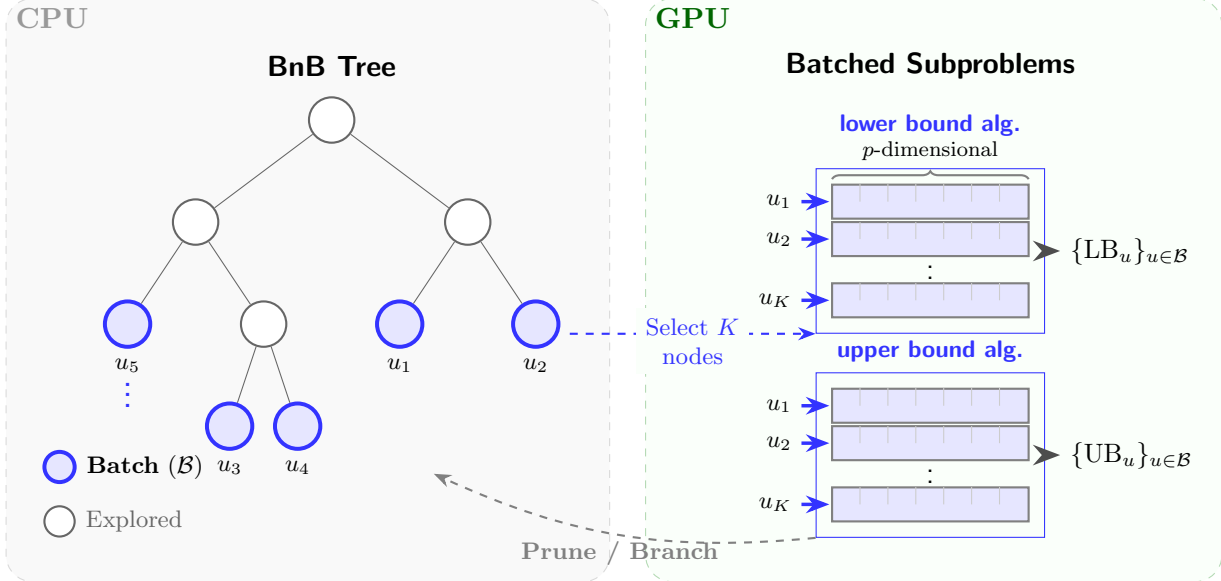


Figure 1: High-level view of our GPU-accelerated BnB algorithm. A batch \mathcal{B} of K active nodes from the CPU-side BnB tree is mapped to batched node subproblem algorithms on the GPU. Each node $u \in \mathcal{B}$ is solved in parallel and the resulting lower (LB_u) and upper bounds (UB_u) are fed back to guide branching and pruning decisions on CPU.

Contributions

Our contributions in the paper are as follows:

- At the core of our BnB framework is a node relaxation algorithm that is highly amenable to parallel computation. By introducing auxiliary and dual variables, we decompose each BnB node subproblem into components that can be solved independently via the Alternating Direction Method of Multipliers (ADMM) algorithm [14]. We choose the ADMM splitting such that the solution to each of the resulting ADMM subproblems are computed in closed-form and highly parallel, meaning they can be dramatically accelerated on GPUs.
- We leverage the separability of our node relaxation algorithm to parallelize subproblems across nodes in the BnB tree. Since problem (1) can have an extremely large number of binary variables, this strategy leads to dramatic speed-ups compared to solving nodes sequentially.
- We introduce an upper bound algorithm based on projected gradient descent that quickly generates high-quality feasible solutions. To fully leverage GPU acceleration, this algorithm is also designed to be parallel both within a node and across nodes in the BnB tree.
- Our empirical evaluation demonstrates that our GPU-accelerated BnB algorithm significantly outperforms both commercial solvers and prior custom methods. On large instances (e.g. $n = 10^4$, $p = 10^5$), even without node parallelism GPUBnB achieves a $35\times$ speedup over our CPU implementation (CPUBnB) and a $6\times$ speedup over L0BnB; at this scale, commercial solvers exceed memory limits. Adding node parallelism on top can lead to an up to $25\times$ increase in nodes solved per second, corresponding to much faster solving times.

1.1 Related work

There have been various MIP-based approaches to solve problem (1) as well as the cardinality-constrained version. [11] solve the cardinality-constrained problem to optimality using Gurobi for $n \sim p \sim 10^3$. [12] propose an outer-approximation approach for the same problem by constructing piece-wise lower bounds to the convex objective, which scales to $p \sim 10^4\text{--}10^5$ when n and λ_2 are sufficiently large. [31] propose scalable algorithms to generate high-quality feasible solutions for very large problems, while [33] extend this to solve problems to optimality for $p \sim 10^5$ or larger in a BnB framework. Our approach is in the same algorithmic vein: we retain a BnB-based strategy for certifying optimality, but reformulate the per-node computations to enable parallel execution on GPUs both within node subproblems and across multiple node subproblems, significantly accelerating large-scale instances compared to prior work. Separately, a complementary line of work develops stronger convex relaxations for related mixed-integer quadratic formulations with indicator variables [5, 13].

The use of GPUs more broadly in optimization has gained significant traction, from enhancing local search subroutines or other heuristics within serial algorithms [49] to the development of novel solvers explicitly designed to exploit parallel processing capabilities [3, 55, 1, 45, 50]. One area where GPUs have shown promise is in linear programming solvers [34, 52, 38, 53]. Traditional linear programming algorithms, such as the simplex method, have been highly optimized for serial execution on CPUs, and do not naturally exploit parallelism. Hence, there is development required to gradually replace fast serial algorithms with new parallel algorithms that can better exploit GPU processing capabilities [38]. Similarly, in convex optimization, conic solvers using interior-point methods are typically the go-to general-purpose algorithm, but pose challenges due to the memory requirements of solving the KKT system on GPUs [45]. Moreover, within BnB algorithms, thousands or millions of subproblems may need to be solved, and warm-starting becomes a crucial strategy but is not always exploitable via methods like interior-point algorithms [21]. Here, there is clearly an interplay emerging between algorithmic development and the strengths and weaknesses of the target hardware.

While parallel implementations of BnB algorithms have been studied since the 1990s and before [17], these approaches have largely focused on coarse-grained parallelism using either shared-memory or message-passing systems. Early attempts at fine-grained parallelism were limited by synchronization overhead and memory constraints, making them suitable only for small problem instances [26]. Our work represents (to our knowledge) the first parallel BnB implementation that effectively exploits modern GPU architectures' capabilities, enabling both parallel subproblem solving and parallel node exploration at scale.

2 Preliminaries: MIP Formulation and Branch-and-Bound Solver

This section discusses the MIP formulation of problem (1), and a specialized BnB framework for solving it.

2.1 Perspective formulation with Big-M constraint

We consider a MIP formulation of problem (1), incorporating Big-M constraints and a perspective reformulation [33, 2].

We define a constant $M > 0$ such that an optimal solution β^* of problem (1) satisfies $\|\beta^*\|_\infty \leq M$. Binary variables $z_i, i \in [p]$, are introduced to control whether each β_i is zero, enforced through the constraints $-Mz_i \leq \beta_i \leq Mz_i, i \in [p]$. To reformulate the ridge term $\|\beta\|_2^2$, we introduce auxiliary

continuous variables $s_i \geq 0$ and impose rotated second-order cone constraints $\beta_i^2 \leq s_i z_i$ for each $i \in [p]$. The term $\lambda_2 \|\beta\|_2^2$ is then replaced with $\lambda_2 \sum_{i \in [p]} s_i$. This results in the following perspective reformulation:

$$\begin{aligned} \min_{\beta, z, s} \quad & \frac{1}{2} \|y - X\beta\|_2^2 + \lambda_0 \sum_{i \in [p]} z_i + \lambda_2 \sum_{i \in [p]} s_i \\ \text{s.t.} \quad & -Mz_i \leq \beta_i \leq Mz_i, \quad i \in [p], \\ & \beta_i^2 \leq s_i z_i, \quad i \in [p], \\ & z_i \in \{0, 1\}, s_i \geq 0, \quad i \in [p]. \end{aligned} \tag{2}$$

As long as M is selected appropriately, the perspective formulation (2) remains equivalent to the original problem (1). Practical approaches for estimating M can be found in [11, 59]. Problem (2) is a mixed-integer second-order conic problem, and when the binary variable is relaxed to $z \in [0, 1]$, it becomes a second-order conic problem.

2.2 Overview of our Custom Branch-and-Bound framework

In this section, we present an overview of our BnB framework for solving problem (2). We first outline the parts of our BnB framework which align with traditional BnB, and then how we design our subproblem solvers to take advantage of parallelism in the BnB tree. In Section 3, we describe in more detail how we design the components can be accelerated with GPUs.

2.2.1 Traditional Branch-and-Bound

The core principle of BnB is to systematically explore the solution space by dividing it into smaller subproblems (branching) and eliminating parts of the search space that cannot contain the optimal solution (bounding). We briefly outline the components of our algorithm below, which resemble a typical BnB procedure:

- **Binary branching.** For problem (2), each subproblem of the solution space can be represented by two sets, $(\mathcal{F}_0, \mathcal{F}_1)$, which correspond to solving the problem with additional constraints: $z_i = 0$ for all $i \in \mathcal{F}_0$ and $z_i = 1$ for all $i \in \mathcal{F}_1$. The BnB framework explores the solution space using a binary tree structure. It begins at the root node, where the subproblem is $(\mathcal{F}_0, \mathcal{F}_1) = (\emptyset, \emptyset)$. For branching, the algorithm selects a variable, say $j \in [p]$, for the current node and creates two new nodes: one with $(\mathcal{F}_0 \cup \{j\}, \mathcal{F}_1)$ and another with $(\mathcal{F}_0, \mathcal{F}_1 \cup \{j\})$.
- **Node relaxation algorithm (lower bounds).** At each node, we solve an interval relaxation subproblem to obtain a lower bound on the best achievable objective within that node. This relaxation provides the dual (lower) bound used to decide whether a subproblem and its descendants can be safely discarded.
- **Upper-bound algorithm (primal solutions).** An upper-bound solver quickly computes an approximate feasible solution for the node, which provides an upper bound to problem (2) as a whole. These feasible solutions update the best-known objective value and thus tighten the global upper bound.
- **Pruning and search strategy.** To reduce the search tree size, BnB prunes nodes under two conditions: (i) if the lower-bound solver at the current node produces an integer solution for z or (ii) if the node's lower bound exceeds the best-known upper bound. While various node selection strategies can be used (e.g., breadth-first search or depth-first search), we adopt a best-first node selection strategy [37] to accelerate the search further—at each step, BnB selects the node or nodes with the smallest lower bound to solve.

- **Global lower bound and termination.** The global lower bound for the BnB tree is defined as the smallest lower bound among all open leaf nodes. As the algorithm progresses, the global lower bound converges to the optimal objective of problem (2). However, in practice, the algorithm can be terminated early if the gap between the best upper and lower bounds falls below a predefined threshold.

2.3 Parallel Node Subproblem Solver

At each node in the BnB tree, we compute both an upper bound and a lower bound relaxation of problem (2). These are typically the most computationally intensive portions of any BnB algorithm, being the great majority of the overall runtime. Our framework employs two specialized algorithms designed for parallel computation: an ADMM-based lower bound algorithm and a projected gradient descent upper bound algorithm. These algorithms are structured to enable parallel computation across the coordinates of the optimization variables, making them highly efficient on GPU architectures. The ADMM algorithm, detailed in Section 3.1, decomposes the problem into subproblems that can be solved in parallel on GPUs. Similarly, the upper bound algorithm detailed in Section 3.3 operates on the entire support simultaneously rather than cycling through the decision variables.

2.4 Parallel Tree Exploration

As noted in the previous subsections, our ADMM-based node relaxation and proximal-gradient upper bound algorithms are explicitly designed to support parallelism within a subproblem. However, a key feature of our approach is that the very same structure also enables parallelism across nodes in the BnB tree, via the batched implementations we describe in Sections 3.2 and 3.4. Thus an important consideration in our parallel BnB framework is to organize the tree search so that many node subproblems can be processed concurrently on the GPU.

Although BnB is inherently sequential since node selection, branching, and pruning depend on global bounds, we circumvent this bottleneck by decoupling the tree logic from the computationally heavy work done at each node. At each iteration, the CPU uses the current global bounds to select a batch \mathcal{B} of up to K active nodes. Conditional on this snapshot, their relaxations and feasible-solutions are computed in parallel on the GPU. Once the batched solves return, the CPU updates the global bounds and repeats. The overall procedure is summarized in Algorithm 1.

Algorithm 1 Overview of our parallel BnB algorithm. The computationally intensive node subproblems are solved in parallel, indicated in **blue**, while the lightweight serial BnB logic remains unchanged.

Require: Batch K , inputs; **Init** $\mathcal{N} \leftarrow \{u_0\}$, $\text{UB} \leftarrow \infty$, $\text{LB} \leftarrow -\infty$

- 1: **while** $\mathcal{N} \neq \emptyset$ and $(\text{UB} - \text{LB})/\text{UB} > \text{tol}$ **do**
- 2: **Select nodes** $\mathcal{B} \subseteq \mathcal{N}$ $(\min(K, |\mathcal{N}|))$ & **solve for** $\{\text{LB}_u, \text{UB}_u, \beta_u^{\text{feas}}\}_{u \in \mathcal{B}}$ **in parallel**
- 3: **for** each $u \in \mathcal{B}$ **do**
- 4: **if** $\text{LB}_u \geq \text{UB}$ **then** Prune node u ; **continue**
- 5: **if** $\text{UB}_u < \text{UB}$ **then** $\text{UB} \leftarrow \text{UB}_u$, $\beta^* \leftarrow \beta_u^{\text{feas}}$
- 6: Select $j \in [p] \setminus (\mathcal{F}_0 \cup \mathcal{F}_1)$; Add $(\mathcal{F}_0 \cup \{j\}, \mathcal{F}_1, \text{LB}_u)$ and $(\mathcal{F}_0, \mathcal{F}_1 \cup \{j\}, \text{LB}_u)$ to \mathcal{N}
- 7: **end for**
- 8: Update global lower bound $\text{LB} \leftarrow \min\{\text{LB}_u : u \in \mathcal{N}\}$
- 9: **end while**
- 10: **return** β^*

3 Branch-and-Bound Algorithm Components

In this section, we describe the various components of our BnB algorithm in detail. Our goal is to design algorithms that are highly parallel, in contrast to the more serial algorithms introduced in prior work. This approach allows us to leverage the computational power of modern GPUs for finding optimal or near-optimal solutions to problem (1). To this end, we develop two key components:

- An ADMM-based node relaxation algorithm which fully separates across the elements of the decision variables for each subproblem and across subproblems. A key feature in our approach is that these two forms of parallelism are integrated.
- A proximal gradient based upper bound algorithm designed to operate over the entire support at a given node, rather than cycling through the decision variables sequentially.

We first describe how parallelism can be implemented within a node, via our ADMM-based node relaxation and proximal gradient upper-bound algorithms (Sections 3.1 and 3.3), and then how to extend to parallelism across nodes in the BnB tree (Sections 3.2 and 3.4).

3.1 ADMM-based algorithm for the node relaxations

In this section, we propose an ADMM method for solving the relaxation problem (2), which completely separates across the coordinates of each subproblem. Here we describe the ADMM algorithm at a particular node, while parallelism across nodes is discussed in subsection 3.2. At a given node of the BnB tree whose corresponding upper and lower bounds are $(\mathcal{F}_0, \mathcal{F}_1)$, the interval relaxation of the subproblem reads:

$$\begin{aligned} \min_{\beta, z, s} \quad & \frac{1}{2} \|y - X\beta\|_2^2 + \lambda_0 \sum_{i \in [p]} z_i + \lambda_2 \sum_{i \in [p]} s_i \\ \text{s.t.} \quad & \beta_i^2 \leq s_i z_i, \quad i \in [p] \\ & -M z_i \leq \beta_i \leq M z_i, \quad i \in [p] \\ & z_i \in [0, 1], s_i \geq 0, \quad i \in [p] \\ & z_i = 0 \forall i \in \mathcal{F}_0, \quad z_i = 1 \forall i \in \mathcal{F}_1. \end{aligned} \tag{3}$$

To simplify the problem, we use the fact that for a fixed β , the optimal values of s and z can be computed analytically (see Appendix A for detailed derivations). Substituting the optimal values back into the objective function in terms of β , we obtain an equivalent problem that depends only on β :

$$\begin{aligned} \min_{\beta \in \mathbb{R}^p} \quad & \frac{1}{2} \|y - X\beta\|_2^2 + \sum_{i \in [p]} \psi_i(\beta_i; \lambda_0, \lambda_2, M) \\ \text{s.t.} \quad & \|\beta\|_\infty \leq M \end{aligned} \tag{4}$$

where

$$\psi_i(\beta_i; \lambda_0, \lambda_2, M) = \begin{cases} \infty \cdot \mathbf{1}_{\{\beta_i=0\}} & \text{if } i \in \mathcal{F}_0 \\ \lambda_0 + \lambda_2 \beta_i^2 & \text{else if } i \in \mathcal{F}_1 \text{ or } \sqrt{\frac{\lambda_0}{\lambda_2}} \leq |\beta_i| \leq M \\ 2\sqrt{\lambda_0 \lambda_2} |\beta_i| & \text{else if } |\beta_i| \leq \sqrt{\frac{\lambda_0}{\lambda_2}} \leq M \\ (\lambda_0/M + \lambda_2 M) |\beta_i| & \text{else if } \sqrt{\frac{\lambda_0}{\lambda_2}} > M \end{cases} \tag{5}$$

Solving problem (4) using ADMM involves a choice of splitting technique; that is, a choice of auxiliary variable to decouple the problem. We reformulate problem (4) by introducing a copy b of the primal variable β :

$$\begin{aligned} \min_{b, \beta \in \mathbb{R}^p} \quad & \frac{1}{2} \|y - Xb\|_2^2 + \sum_{i \in [p]} \psi_i(\beta_i; \lambda_0, \lambda_2, M) + \infty \cdot \mathbf{1}_{\{\|\beta\|_\infty \leq M\}} \\ \text{s.t.} \quad & b = \beta \end{aligned} \quad (6)$$

Here there are various splittings that could have been used. For example, a popular splitting is to introduce an auxiliary variable $r = y - X\beta$ (c.f. [14], pg 39). However, this leads to coupled updates involving $X\beta$ that cannot be solved completely in parallel. By decoupling b and β , we separate the smooth quadratic term involving b from the non-smooth regularization involving β , such that both resulting subproblems can be parallelized. The constraint $b = \beta$ ensures consistency between the variables. ADMM [14, 18] is a powerful iterative first-order optimization method well-suited for problems with such a structure. It considers the augmented Lagrangian function of this problem that enforces the equality constraint using a dual variable $v \in \mathbb{R}^p$ and a penalty parameter $\rho > 0$:

$$\begin{aligned} \min_{b, \beta \in \mathbb{R}^p} \quad & L_\rho(b, \beta, v) = \frac{1}{2} \|y - Xb\|_2^2 + \sum_{i \in [p]} \psi_i(\beta_i; \lambda_0, \lambda_2, M) \\ & + \infty \cdot \mathbf{1}_{\{\|\beta\|_\infty \leq M\}} + v^\top(b - \beta) + \frac{\rho}{2} \|b - \beta\|_2^2 \end{aligned} \quad (7)$$

The ADMM algorithm proceeds by iteratively minimizing the augmented Lagrangian with respect to primal variables b and β , and dual variable v . Specifically, at iteration t , the updates are:

$$\begin{aligned} b^{(t+1)} &= \arg \min_b L_\rho(b, \beta^{(t)}, v^{(t)}) \\ \beta^{(t+1)} &= \arg \min_\beta L_\rho(b^{(t+1)}, \beta, v^{(t)}) \\ v^{(t+1)} &= \arg \min_v L_\rho(b^{(t+1)}, \beta^{(t+1)}, v) \end{aligned} \quad (8)$$

3.1.1 Structuring the ADMM updates to exploit parallelism

We now describe how the solution to each subproblem can be computed in a separable fashion.

Update for b . To update of $b^{(t+1)}$ in (8), we solve the optimization problem:

$$b^{(t+1)} = \arg \min_b \left\{ \frac{1}{2} \|y - Xb\|_2^2 + v^{(t)\top}(b - \beta^{(t)}) + \frac{\rho}{2} \|b - \beta^{(t)}\|_2^2 \right\}. \quad (9)$$

$$= \left(X^\top X + \rho I \right)^{-1} \left(X^\top y + \rho \beta^{(t)} - v^{(t)} \right) \quad (10)$$

At first glance this update appears to couple the coordinates of b . However, notice that we can precompute the matrix $D = (X^\top X + \rho I)^{-1}$ and the vector $c = X^\top y$ before the ADMM iterations begin. When p is much larger than n (e.g. $p \sim 10^5$, $n \sim 10^3$), inverting this matrix can be expensive. However, we can exploit the equivalent reformulation of the inverse:

$$D = \begin{cases} (X^\top X + \rho I_p)^{-1} & \text{if } n \geq p, \\ \frac{1}{\rho} I_p - \frac{1}{\rho^2} X^\top (X X^\top + \rho I_n)^{-1} X & \text{if } p > n. \end{cases}$$

When $X^\top X$ is a large matrix of size $p \times p$, it is more efficient to compute D to use the Sherman-Morrison-Woodbury formula [29], as it only involves inverting an $n \times n$ matrix. Moreover, efficient

matrix factorization routines reduce the inversion problem to solving two triangular systems via forward and backward substitution, each with $\mathcal{O}(n^2)$ complexity. Importantly, this precomputation of D only needs to be done once for the *entire tree* in BnB. Once D and c are precomputed, the per-iteration computation of $b^{(t+1)}$ reduces to operations involving vectors, and the update can be parallelized. Specifically, for each coordinate i :

$$b_i^{(t+1)} = \sum_{j=1}^p D_{ij} \left(c_j + \rho \beta_j^{(t)} - v_j^{(t)} \right), \quad \text{for } i = 1, \dots, p \quad (11)$$

hence, each coordinate b_i can be assigned a unique thread and computed independently.

Update for β . The update for $\beta^{(t+1)}$ in (8) is inherently separable and can be computed in closed form for each coordinate $i \in [p]$ as:

$$\begin{aligned} \beta_i^{(t+1)} &= \arg \min_{\beta_i} \frac{\rho}{2} (\beta_i - \tilde{\beta}_i)^2 + \psi_i(\beta_i; \lambda_0, \lambda_2, M) + \infty \cdot \mathbf{1}_{\{\beta_i \leq M\}} \\ &= \begin{cases} 0 & \text{if } i \in \mathcal{F}_0 \\ T\left(\frac{\rho}{\rho+2\lambda_2}\tilde{\beta}_i, 0, M\right) & \text{else if } i \in \mathcal{F}_1 \text{ or } \frac{2\sqrt{\lambda_0\lambda_2}}{\rho} + \sqrt{\frac{\lambda_0}{\lambda_2}} \leq |\tilde{\beta}_i| \\ T\left(\tilde{\beta}_i; \frac{2\sqrt{\lambda_0\lambda_2}}{\rho}, M\right) & \text{else if } |\tilde{\beta}_i| \leq \frac{2\sqrt{\lambda_0\lambda_2}}{\rho} + \sqrt{\frac{\lambda_0}{\lambda_2}}, \sqrt{\frac{\lambda_0}{\lambda_2}} \leq M \\ T\left(\tilde{\beta}_i; \frac{\lambda_0}{M\rho} + \frac{\lambda_2 M}{\rho}, M\right) & \text{else if } \sqrt{\frac{\lambda_0}{\lambda_2}} > M \end{cases} \end{aligned} \quad (12)$$

where $\tilde{\beta}_i = b_i + v_i/\rho$ and $T : \mathbb{R} \rightarrow \mathbb{R}$ denotes the box-constrained soft-thresholding operator

$$T(t; a, m) := \begin{cases} 0 & \text{if } |t| \leq a \\ (|t| - a) \text{ sign}(t) & \text{if } a < |t| \leq a + m \\ m \text{ sign}(t) & \text{otherwise} \end{cases} \quad (13)$$

The solution in (12) comes from reasoning about the different cases of the piece-wise function in (5). The derivations are given in Appendix A. The coordinate is either zero (if i belongs to the upper bound set \mathcal{F}_0) or is the result of a thresholding operation. These thresholding operations can be batched efficiently across the coordinates in popular libraries for GPU-accelerated computation, such as PyTorch. See Algorithm 2 for pseudo code utilizing native PyTorch vectorized operations.

Algorithm 2 PyTorch code for β -update

```

# Inputs:
#   -  $\tilde{\beta}$ : tensor of shape (p)
#   -  $\lambda_0, \lambda_2, \rho, M$ : scalars
#   -  $a$ : tensor of shape (p) of thresholds for each  $i$ 
#   -  $\mathcal{F}_0, \mathcal{F}_1$ : boolean masks of shape (p)

def beta_update(beta, lambda_0, lambda_2, rho, M, a, F0, F1):
    beta_F1 = (rho / (rho + 2 * lambda_2)) * beta
    beta_F1 = beta_F1.clamp(-M, M)
    beta_remain = torch.sign(beta) * torch.clamp(torch.abs(beta) - a, min=0.0)
    beta_remain = beta_remain.clamp(-M, M)
    beta = torch.where(F0, torch.zeros_like(beta),
                      torch.where(F1, beta_F1, beta_remain))
    return beta

```

Update for v . Finally, we can also see that the update for v in (8) is separable across the coordinates because each component v_i depends only on the corresponding components b_i and β_i :

$$v_i^{(t+1)} = v_i^{(t)} + \rho \left(b_i^{(t+1)} - \beta_i^{(t+1)} \right), \quad \text{for } i = 1, \dots, p. \quad (14)$$

where, similar to the update for b , each coordinate can be assigned a unique thread and computed in parallel.

Overall, these updates align well with the Same Instruction Multiple Data (SIMD) programming model of GPUs, where many parallel elements are processed independently using the same program [44]. Figure 2 illustrates the ADMM updates used in our framework. As shown in the figure, ADMM allows for operator splitting by separating the optimization problem into sequential updates of primal variables b , auxiliary variables β , and dual variables v . These updates can be computed in closed-form and decomposed across the elements of each vector for fast parallel computation, as depicted in the right-hand side of Figure 2. This coordinate-wise decomposition enables fast parallel updates on GPUs, making our subproblem algorithm highly efficient for large-scale problems.

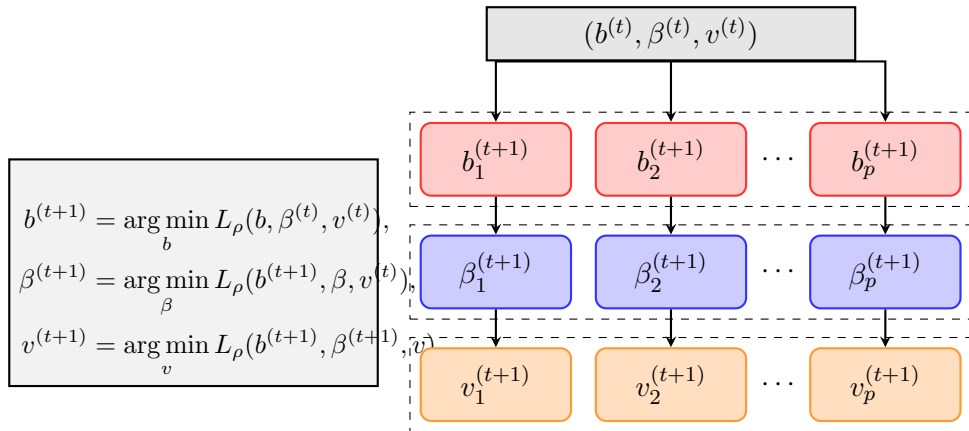


Figure 2: Illustration of the Alternating Direction Method of Multipliers (ADMM) updates. **Left:** ADMM allows for operator splitting by separating the optimization problem into sequential updates of primal variables b , auxiliary variables β , and dual variables v . Each variable is updated by minimizing the augmented Lagrangian L_ρ with respect to that variable while keeping the others fixed. **Right:** These updates can be decomposed across the coordinates of all vectors for fast parallel computation. Each component $b_i^{(t+1)}$, $\beta_i^{(t+1)}$, $v_i^{(t+1)}$ for $i = 1, \dots, p$ is updated independently across coordinates, which enables fast parallel updates on GPUs.

3.1.2 Dual Bounds

Our ADMM-based lower bound algorithm is iterative and produces inexact primal solutions to problem (6) in practice, which may not provide a valid lower bound. To ensure that our BnB framework prunes the search space correctly, we need the dual bound of problem (6). We first present a dual of Problem (6) and its optimality conditions in the following theorem.

Proposition 1. *We define function $h : \mathbb{R}_{\geq 0} \rightarrow \mathbb{R}$ as*

$$h(x) = \begin{cases} x^2/4\lambda_2 - \lambda_0 & \text{if } x \leq 2M\lambda_2 \\ Mx - \lambda_0 - \lambda_2 M^2 & \text{otherwise.} \end{cases} \quad (15)$$

A dual of problem (6) is then given by

$$\max_{r \in \mathbb{R}^n} -\frac{1}{2} \|r\|_2^2 + y^\top r - \sum_{i \in [p]} \nu_i (|X_i^\top r|) \quad (16)$$

where

$$\nu_i(x) = \begin{cases} 0 & \text{if } i \in \mathcal{F}_0 \\ h(x) & \text{else if } i \in \mathcal{F}_1 \\ [h(x)]_+ & \text{else if } \sqrt{\frac{\lambda_0}{\lambda_2}} \leq M \\ [Mx - \lambda_0 - \lambda_2^2]_+ & \text{else if } \sqrt{\frac{\lambda_0}{\lambda_2}} > M \end{cases} \quad (17)$$

Let (b^*, β^*) be an optimal solution to problem (6), then $r^* = y - Xb^*$ is the optimal dual solution of problem (16). Moreover, strong duality holds for (6).

Motivated by the optimality condition provided in Theorem 1, given an inexact primal solution $(\hat{b}, \hat{\beta})$ obtained from ADMM, we set $\hat{r} = y - X\hat{b}$ as the approximate dual solution. It is worth noting that similar to the update of β in ADMM, the computation of the dual bound can exploit GPU acceleration.

3.1.3 ADMM Warm Starting.

For the root node, we initialize the ADMM variables to zero. For child nodes, we warm-start from the parent solution, modifying the iterates to respect the newly fixed coordinates in \mathcal{F}_0 and \mathcal{F}_1 (e.g., setting $\beta_i = 0$ for $i \in \mathcal{F}_0$), and then updating b and v via (11) and (14). Since a child differs from its parent only by a small number of additional fixings, this typically provides a strong initialization and substantially reduces the number of ADMM iterations per node. This is a key advantage of ADMM as a first-order method in branch-and-bound. The optimization variables (b, β, v) transfer directly across related nodes, and the matrix D is reused across the entire tree. By contrast, interior-point methods are generally less effective at exploiting warm-starts when constraints change, so they tend to require more work per node even when successive subproblems are very similar [45].

3.2 Parallelizing the Lower Bound Algorithm Across the BnB Tree

In solving mixed-integer optimization problems via BnB algorithms with many binary variables, such as (2), a key challenge is efficiently traversing the many subproblems that arise via branching. Each node in the BnB tree represents a subproblem defined by specific variable fixations, and as the tree expands, the number of open nodes (i.e., subproblems yet to be solved) can grow exponentially. In this section, we discuss how we leverage the structure of our problem to parallelize computations across several open nodes in the search tree.

Consider K subproblems corresponding to different open nodes in the BnB tree. Each subproblem $k \in [K]$ is characterized by its own fixed sets $\mathcal{F}_0^{(k)}$ and $\mathcal{F}_1^{(k)}$, which represent variables fixed to zero or one, respectively. The goal is to solve these subproblems simultaneously by batching their ADMM updates. For parallel computation, we represent the variables across all subproblems using batched matrices:

- $B \in \mathbb{R}^{K \times p}$: Batch of primal variables $\{b^{(k)}\}_{k=1}^K$
- $\beta \in \mathbb{R}^{K \times p}$: Batch of auxiliary variables $\{\beta^{(k)}\}_{k=1}^K$
- $V \in \mathbb{R}^{K \times p}$: Batch of dual variables $\{v^{(k)}\}_{k=1}^K$

Each row $k \in [K]$ in these matrices corresponds to the variables of subproblem k , allowing us to perform operations across all subproblems simultaneously, as depicted in Figure 2

Update for B . The primal update for all subproblems can be computed as

$$B^{(t+1)} = (C + \rho \beta^{(t)} - V^{(t)}) D, \quad (18)$$

where $D = (X^\top X + \rho I_p)^{-1} \in \mathbb{R}^{p \times p}$ is precomputed and $C := \mathbf{1}_K (X^\top y)^\top \in \mathbb{R}^{K \times p}$ is the matrix whose k -th row equals $(X^\top y)^\top$, with $\mathbf{1}_K \in \mathbb{R}^K$ being a K -dimensional vector with 1 at every entry. In other words, C replicates the vector $X^\top y$ across the K subproblems. For efficient storage, we implement a shared memory reference such that we only store $X^\top y$ itself.

Update for β . The update for β applies the proximal operator T element-wise:

$$\beta_{k,i}^{(t+1)} = T(\tilde{\beta}_{k,i}; a_{k,i}, M), \quad (19)$$

where $\tilde{\beta} = B^{(t+1)} + \frac{V^{(t)}}{\rho}$, and $a_{k,i}$ and $m_{k,i}$ are parameters that depend on the fixations in $\mathcal{F}_0^{(k)}$ and $\mathcal{F}_1^{(k)}$ for each subproblem k . To efficiently implement this update on GPUs, it is essential to define masks for each subproblem k and coordinate i :

$$\delta_{k,i}^{(0)} = \begin{cases} 1, & \text{if } i \in \mathcal{F}_0^{(k)}, \\ 0, & \text{otherwise;} \end{cases} \quad \delta_{k,i}^{(1)} = \begin{cases} 1, & \text{if } i \in \mathcal{F}_1^{(k)}, \\ 0, & \text{otherwise;} \end{cases} \quad \delta_{k,i}^{(f)} = 1 - \delta_{k,i}^{(0)} - \delta_{k,i}^{(1)}.$$

Using these masks, we express the auxiliary variable update for all subproblems and coordinates in vectorized form as:

$$\beta^{(t+1)} = \delta^{(0)} \circ \mathbf{0} + \delta^{(1)} \circ \beta_{\text{fixed}}^{(t+1)} + \delta^{(f)} \circ \beta_{\text{free}}^{(t+1)}, \quad (20)$$

where “ \circ ” denotes element-wise multiplication. $\beta_{\text{fixed}}^{(t+1)} \in \mathbb{R}^{K \times p}$ is the update for variables fixed to one, computed as:

$$\beta_{\text{fixed}}^{(t+1)} = \text{proj}_{[-M, M]} \left(\frac{\rho}{\rho + 2\lambda_2} \tilde{\beta} \right).$$

$\beta_{\text{free}}^{(t+1)} \in \mathbb{R}^{K \times p}$ is the update for free variables, computed using the proximal operator T :

$$\beta_{\text{free},k,i}^{(t+1)} = \begin{cases} T \left(\tilde{\beta}_{k,i}; \frac{2\sqrt{\lambda_0 \lambda_2}}{\rho}, M \right), & \text{if } \sqrt{\frac{\lambda_0}{\lambda_2}} \leq M, \\ T \left(\tilde{\beta}_{k,i}; \frac{\lambda_0}{M\rho} + \frac{\lambda_2 M}{\rho}, M \right), & \text{if } \sqrt{\frac{\lambda_0}{\lambda_2}} > M. \end{cases}$$

The use of binary masks to handle variable fixations is very well-suited for GPU acceleration. Rather than explicitly maintaining different sets of active variables for each subproblem, the masks allow us to compute updates for all variables and then efficiently zero out or modify values based on their fixed status. This approach avoids conditional branches in the GPU code, which could otherwise lead to thread divergence and reduce performance.

Update for V . The dual variables V are updated simultaneously for all subproblems in vectorized form:

$$V^{(t+1)} = V^{(t)} + \rho (B^{(t+1)} - \beta^{(t+1)}) \quad (21)$$

This batched formulation in equations (18)-(21) offers several key advantages. First, it allows us to leverage the high throughput of modern GPUs by processing multiple subproblems simultaneously

using common instructions (see Figure 3). The matrix operations can be efficiently computed using GPU-optimized linear algebra libraries. Second, all subproblems share the same data matrix X at the matrix D , to avoid memory consumption becoming a bottleneck on GPUs. As discussed in subsection 4.4, this batched formulation can process far more nodes in parallel and drastically reduces the time to close the optimality gap.

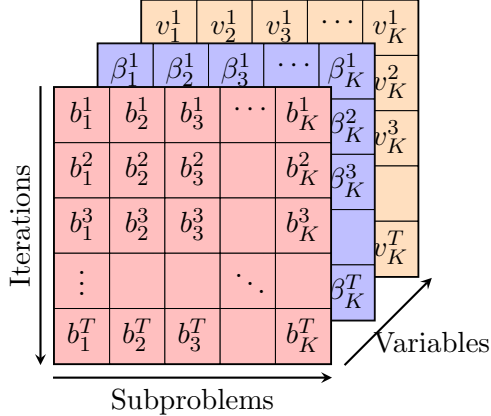


Figure 3: SIMD model for parallel lower bound algorithm

Our shared memory reference scheme exploits a key observation: in the branch-and-bound tree, all subproblems operate on the same underlying data matrices (X , D and y), with differences only in the variables b , β , and v . Instead of naively replicating these matrices for each subproblem, which would quickly exhaust GPU memory, we maintain a single global reference to these common data. Each subproblem stores only its unique decision variables.

3.3 Upper bound algorithm

Throughout the BnB algorithm execution, whenever we find an integral solution, its cost serves as an upper bound for the original problem's optimal solution. Upper bounds are critical in BnB algorithms for efficiently pruning the search space and avoiding exhaustive enumeration. This section discusses how to get a feasible solution for problem (2) efficiently. Given a solution $(\hat{\beta}, \hat{z}, \hat{s})$ of the relaxation problem (3), we round each component of \hat{z} to get an integral solution z^* . With fixed $z = z^*$, problem (2) reduces to a quadratic problem with box constraint:

$$\begin{aligned} \min_{\beta_S} \quad & U_S(\beta_S) := \frac{1}{2} \|y - X_S \beta_S\|_2^2 + \lambda_2 \|\beta_S\|_2^2 \\ \text{s.t.} \quad & |\beta_i| \leq M, \quad i \in \mathcal{S}, \end{aligned} \tag{22}$$

where X_S denotes the submatrix of X with columns in $\mathcal{S} = \{i \mid z_i = 1\}$. We solve (22) using a fast proximal gradient method with Nesterov acceleration and backtracking line search. At iteration t , given the current and previous iterates $\beta_S^{(t)}$ and $\beta_S^{(t-1)}$, we first form an extrapolated point

$$\tilde{\beta}_S^{(t)} = \beta_S^{(t)} + \frac{t}{t+3} (\beta_S^{(t)} - \beta_S^{(t-1)}), \tag{23}$$

then compute the gradient of the smooth part:

$$\nabla g(\tilde{\beta}_S^{(t)}) = X_S^\top (X_S \tilde{\beta}_S^{(t)} - y) + 2\lambda_2 \tilde{\beta}_S^{(t)}, \tag{24}$$

and form a projected gradient step with stepsize $\alpha^{(t)}$:

$$\beta_{\mathcal{S}}^{(t+1)} = \Pi_{[-M,M]} \left(\tilde{\beta}_{\mathcal{S}}^{(t)} - \alpha^{(t)} \nabla g(\tilde{\beta}_{\mathcal{S}}^{(t)}) \right), \quad (25)$$

where $\Pi_{[-M,M]}$ denotes the elementwise projection onto $[-M, M]$. The stepsize $\alpha^{(t)}$ is chosen via a standard backtracking line search: we shrink $\alpha^{(t)}$ until the Armijo condition:

$$U_{\mathcal{S}}(\beta_{\mathcal{S}}^{(t+1)}) \leq U_{\mathcal{S}}(\tilde{\beta}_{\mathcal{S}}^{(t)}) + \langle \nabla g(\tilde{\beta}_{\mathcal{S}}^{(t)}), \beta_{\mathcal{S}}^{(t+1)} - \tilde{\beta}_{\mathcal{S}}^{(t)} \rangle + \frac{1}{2\alpha^{(t)}} \|\beta_{\mathcal{S}}^{(t+1)} - \tilde{\beta}_{\mathcal{S}}^{(t)}\|_2^2 \quad (26)$$

is satisfied. The procedure is terminated when the decrease in $U_{\mathcal{S}}$ or the change in $\beta_{\mathcal{S}}$ falls below a prescribed tolerance, at which point the resulting $\beta_{\mathcal{S}}$ provides a feasible upper bound for the original problem.

3.4 Parallelizing the upper bound algorithm across the BnB tree

To efficiently handle many candidate supports in parallel, we implement a vectorized version of the fast proximal gradient scheme in (23)–(26) that, similar to the algorithm presented in subsection 3.2, can handle K problems in parallel. Instead of solving (22) separately for each support, we stack all coefficient vectors into a single matrix $\mathbf{B} \in \mathbb{R}^{K \times p}$, where row k corresponds to subproblem k , and encode the supports via a binary mask $\mathbf{M} \in \{0, 1\}^{K \times p}$, with $\mathbf{M}_{k,j} = 1$ if $j \in \mathcal{S}^k$ and 0 otherwise.

Each iteration applies the extrapolation step (23) in a batched fashion:

$$\tilde{\mathbf{B}}^{(t)} = \mathbf{B}^{(t)} + \frac{t}{t+3} (\mathbf{B}^{(t)} - \mathbf{B}^{(t-1)}),$$

which is simply (23) applied row-wise to $\mathbf{B}^{(t)}$. We then compute all gradients simultaneously, in analogy with (24), via:

$$\nabla G(\tilde{\mathbf{B}}^{(t)}) = (\mathbf{X}^\top (\mathbf{X} \tilde{\mathbf{B}}^{(t)\top} - \mathbf{y} \mathbf{1}^\top))^\top + 2\lambda_2 \tilde{\mathbf{B}}^{(t)},$$

and enforce the support constraints by elementwise masking $\nabla G \leftarrow \nabla G \odot \mathbf{M}$. The projected gradient step (25) is likewise applied in one shot to all rows:

$$\mathbf{B}^{(t+1)} = \Pi_{[-M,M]} (\tilde{\mathbf{B}}^{(t)} - \boldsymbol{\alpha} \odot \nabla G(\tilde{\mathbf{B}}^{(t)})) \odot \mathbf{M},$$

where $\boldsymbol{\alpha} \in \mathbb{R}^K$ stores per-subproblem stepsizes and \odot denotes broadcasting and elementwise multiplication over rows.

Finally, the backtracking line search enforces a batched version of the Armijo condition (26): we maintain a boolean “active” mask over subproblems, update only the active rows of \mathbf{B} and $\boldsymbol{\alpha}$, and evaluate all corresponding trial losses via batched matrix–matrix products until the inequality in (26) holds for each active row. These updates are therefore direct vectorized analogues of (23)–(26), yielding a highly parallel upper-bound algorithm that can process large batches of supports from the B&B tree in a single pass.

3.5 Initializing the BnB tree with specialized heuristic

The upper bound algorithm above is used to quickly obtain a feasible solution given a pre-specified support. This algorithm is highly efficient to run at every node, but relies on the support being high quality. Thus we also design a heuristic algorithm to generate a high-quality support prior to running the BnB algorithm, starting from scratch. This provides a high-quality upper bound prior to initialize the BnB algorithm. The algorithm is a matching pursuit-inspired algorithm (aka greedy selection [22]) with forward and backward phases, and also exploits GPU acceleration during candidate evaluation. We provide more details of the algorithm in subsection A.2.

3.6 Considerations and Challenges for BnB on GPUs

While GPUs have great promise in BnB, they also bring unique challenges and considerations. We outline below some challenges we have encountered with integrating BnB on GPUs and how we address them.

Modes of parallelism. GPUs are highly optimized for SIMD operations, where the same or similar instructions are executed concurrently on multiple threads. If the operations are highly dissimilar this can lead to thread divergence, i.e. a situation in which the same group of threads take different execution paths which forces serialization. The choice of subproblem algorithm itself determines the degree of parallelism that can be achieved. While algorithms like coordinate descent may be more efficient for CPU execution due to their sequential nature, we employ ADMM as it enables decomposition of the problem into subproblems with parallel coordinates. Moreover, we carefully chose the splitting and updates for maximum separability in the coordinate subproblems.

GPU-CPU communication bottlenecks. Transferring large data structures regularly from the CPU to the GPU can introduce communication overhead and slow down the execution of BnB. We have designed our algorithm such that the lightweight serial logic (branching, bounding, pruning, etc) is performed on CPUs while the subproblem algorithms are executed on GPUs (see Algorithm 1). The only data that needs to be passed between the CPU and GPU are the bound evaluations and, when warm starting is used, the decision variables for a given node.

Memory. Modern GPUs typically have 32-96GBs of RAM. If not managed properly, this memory can be exhausted very quickly for large instances. We address this by implementing shared memory references for the vectors and matrices required for the lower-bound and upper-bound algorithms in Section 3. This means the same vectors and matrices (D , X , y) can be reused by each subproblem algorithm.

4 Experiments

This section evaluates our proposed BnB algorithm against state-of-the-art approaches for sparse learning in high-dimensional settings. Our analysis focuses on three aspects: computational efficiency compared to existing methods, sensitivity to parameter settings, and performance across diverse datasets. For section subsection 4.1, we turn off node parallelism to compare with existing BnB methods which also process nodes sequentially. In subsection 4.4, we show that node parallelism further accelerates this algorithm both in terms of the number of nodes processed and the MIP optimality gap.

4.1 Experimental setup

Our algorithm, GPUBnB, is implemented in Python using PyTorch [47] for GPU acceleration via NVIDIA CUDA. We evaluate it on an NVIDIA A100-PCIe-80GB GPU against four baselines: (i) the CPU version of our algorithm (CPUBnB), (ii) L0BnB [33] implemented in Python with Numba optimization [36], and (iii) MOSEK [4]. All CPU-based methods run on 20 AMD EPYC 9474F cores (3.00 GHz, 80GB RAM, 4 threads).

Datasets. For synthetic datasets, following [31, 33], we generate the data matrix $X \in \mathbb{R}^{n \times p}$ by drawing each row from a multivariate Gaussian distribution $\mathcal{N}(0, \Sigma)$, where $\Sigma = \rho \mathbf{1}_{p \times p} + (1 - \rho) \mathbf{I}_p$ controls feature correlation through parameter ρ . The ground truth coefficient $\beta^\dagger \in \mathbb{R}^p$ is constructed with k^0 equispaced nonzero entries of value 1, with remaining entries set to 0. We generate the response vector as $y = X\beta^\dagger + \varepsilon$, where $\varepsilon \sim \mathcal{N}(0, \sigma^2 I_n)$ represents i.i.d. Gaussian noise. The signal-to-noise ratio, defined as $\text{SNR} = \text{Var}(X\beta^\dagger)/\sigma^2$, characterizes problem difficulty: lower SNR

indicates higher noise levels. Unless otherwise specified, we set $\rho = 0.2$, $k^0 = 10$. We adjust SNR based on sample size n : $(\text{SNR}, n) = (10, 1000)$, $(10/3, 3000)$, and $(0.5, 10000)$.

We also evaluate our proposed algorithm on the real-world UJIIndoorLoc dataset [56], which focuses on indoor positioning using WLAN/WiFi fingerprinting across multiple buildings and floors. The dataset is split into training (60%), validation (20%), and test (20%) sets. To create a higher-dimensional problem, we augment the feature space by replicating each feature 49 times with random permutations, resulting in a dataset with $n = 11,962$ samples and $p = 23,250$ features. We preprocess the data by mean-centering and normalizing both the response variable and the feature matrix columns.

Selection of λ_0 , λ_2 , and M . Following [33], for synthetic datasets we first determine λ_2 by analyzing the ridge regression solution restricted to the true support $S^\dagger = \text{supp}(\tilde{\beta}^\dagger)$. Specifically, for fixed λ_2 , we define $\beta(\lambda_2)$ as:

$$\beta(\lambda_2) \in \arg \min_{\beta \in \mathbb{R}^p} \frac{1}{2} \|y - X\beta\|_2^2 + \lambda_2 \|\beta\|_2^2 \quad \text{s.t.} \quad \beta_{(S^\dagger)^c} = 0. \quad (27)$$

The optimal λ_2^* is then determined by minimizing the ℓ_2 estimation error:

$$\lambda_2^* \in \arg \min_{\lambda_2 \geq 0} \|\tilde{\beta}^\dagger - \beta(\lambda_2)\|_2. \quad (28)$$

We estimate λ_2^* through grid search over $[10^{-4}, 10^4]$ using 100 logarithmically-spaced points. In our experiments, we typically set $\lambda_2 = \lambda_2^*$, though we also examine other values as fractions or multiples of λ_2^* .

After determining λ_2 , we follow the adaptive selection rules in [31] to compute a regularization path of decreasing λ_0 values: $\lambda_0^1(\lambda_2) > \lambda_0^2(\lambda_2) > \dots > \lambda_0^m(\lambda_2)$. For each $\lambda_0^i(\lambda_2)$, we apply GPUBnB to solve problem (2) with $\lambda_0 = \lambda_0^i(\lambda_2)$, $\lambda_2 = \lambda_2$, $M = 1.05\|\beta(\lambda_2)\|_\infty$ and a 120 seconds time limit to obtain approximate solution $\hat{\beta}(\lambda_0^i(\lambda_2))$. We select $\lambda_0^*(\lambda_2)$ that maximizes the F-measure between the support of the approximate solution, i.e., $\text{supp}(\hat{\beta}(\lambda_0^i(\lambda_2), \lambda_2))$, and the true support S^\dagger . For the big-M parameter, we set $M^*(\lambda_2) = \|\hat{\beta}(\lambda_2)\|_\infty$. Unless otherwise specified, our experiments use $\lambda_0 = \lambda_0^*(\lambda_2)$ and $M = 1.5M^*(\lambda_2)$.

For real datasets, where the true coefficient vector $\tilde{\beta}^\dagger$ is unknown, we perform a grid search over regularization parameters λ_0 and λ_2 . We select 20 values of λ_2 logarithmically spaced in $[10^{-3}, 10^3]$ and vary λ_0 to obtain solutions with different sparsity levels. For each parameter pair (λ_0, λ_2) , we apply GPUBnB to solve problem (2) with a 120-second time limit, obtaining approximate solution $\hat{\beta}(\lambda_0, \lambda_2)$. The optimal regularization parameters are then selected using the validation set. For the big-M parameter, similarly, we set $M = 1.5\|\hat{\beta}(\lambda_0, \lambda_2)\|_\infty$.

BnB Settings All BnB methods are applied to the perspective formulation (2). For each BnB algorithm, we define the relative optimality gap between the upper bound UB and lower bound LB as $(UB - LB)/UB$. We terminate the algorithm when the relative optimality gap falls below 1% or when reaching either the maximum runtime of 4 hours or the memory limit of 80GB. Additionally, at the node level, we terminate each relaxation subproblem in the BnB tree when its primal-dual gap becomes smaller than 10^{-4} .

4.2 Comparison with state-of-the-art BnB methods on synthetic datasets

4.2.1 Varying number of samples and features

We examine BnB algorithm performance across different problem dimensions. We generate synthetic datasets with varying sizes: the number of samples $n \in \{10^3, 3 \cdot 10^3, 10^4\}$ and the number of features

$p \in \{10^4, 3 \cdot 10^4, 10^5\}$, fixing $k^0 = 10$ nonzeros. Parameters λ_0 , λ_2 , and M are selected as described in Section 4.1. Table 1 presents average runtimes over 10 random seeds for each method.

The results reveal several key findings. First, compared to the commercial solver MOSEK, the other three methods achieve more than 10x speedup for the smallest problem size ($n = 10^3$, $p = 10^4$) and can handle larger instances where MOSEK fails due to memory constraints. Second, comparing the CPU-based methods, L0BnB generally outperforms CPUBnB, especially when the sample-to-feature ratio (n/p) is small, while CPUBnB shows slightly better performance for larger n/p ratios.

Finally, our GPU implementation achieves significant speedups of 5-35x over its CPU counterpart, with the acceleration becoming more significant as the problem size $n \times p$ increases.

n	p	GPUBnB	CPUBnB	L0BnB	MOSEK	GUROBI
10^3	10^4	23.7	149	46.9	1796	-
	$3 \cdot 10^4$	58.4	967	225	-	-
	10^5	355	9182	847	-	-
$3 \cdot 10^3$	10^4	25.7	358	74.8	-	-
	$3 \cdot 10^4$	67.1	1728	177	-	-
	10^5	272	8958	504	-	-
10^4	10^4	9.91	279	328	-	-
	$3 \cdot 10^4$	79.9	2623	688	-	-
	10^5	257	8911	1514	-	-

Table 1: Runtime (in seconds) of our approach versus competing methods averaged over 10 random seeds. ‘-’ indicates an exceeded memory limit (80GB).

We further analyze the performance differences between L0BnB and our approach. Both methods employ identical branch-and-bound frameworks and solve the same MIP problem (2) at each node. In both approaches, over 98% of the runtime is devoted to solving the node relaxation problem (3), with performance differences stemming from their distinct methods: L0BnB uses coordinate descent (CD), while our approach employs ADMM. L0BnB’s CD implementation, as described in [33], incorporates several problem-specific tricks (e.g., active set updates and gradient screening) that enhance its performance. However, the inherently sequential nature of CD makes GPU acceleration challenging. In contrast, our ADMM-based approach, while more general, readily exploits GPU parallelization. Figure 4 compares the average node relaxation solving time between methods across 10 random seeds. While L0BnB outperforms CPUBnB in single-node solution time, our GPU implementation (GPUBnB) achieves a 2-10x speedup compared to L0BnB. Moreover, our approach demonstrates more consistent performance across different seeds.

4.2.2 Impact of problem parameters and computing platforms

We first examine how various problem parameters affect the performance of each BnB method. We generate synthetic datasets with $n = 3000$ samples and $p = 30000$ features. We set baseline parameters $\text{SNR} = 10/3$, $k^0 = 10$, with λ_2 and λ_0 chosen as described in Section 4.1. We then vary one parameter at a time:

- $\text{SNR} \in \{0.5, 1, 2, 3, 10\}$
- $k^0 \in \{5, 10, 15, 20, 25\}$
- $\lambda_2 \in \{0.03, 0.1, 0.3, 3, 10, 30\} \cdot \lambda_2^*$

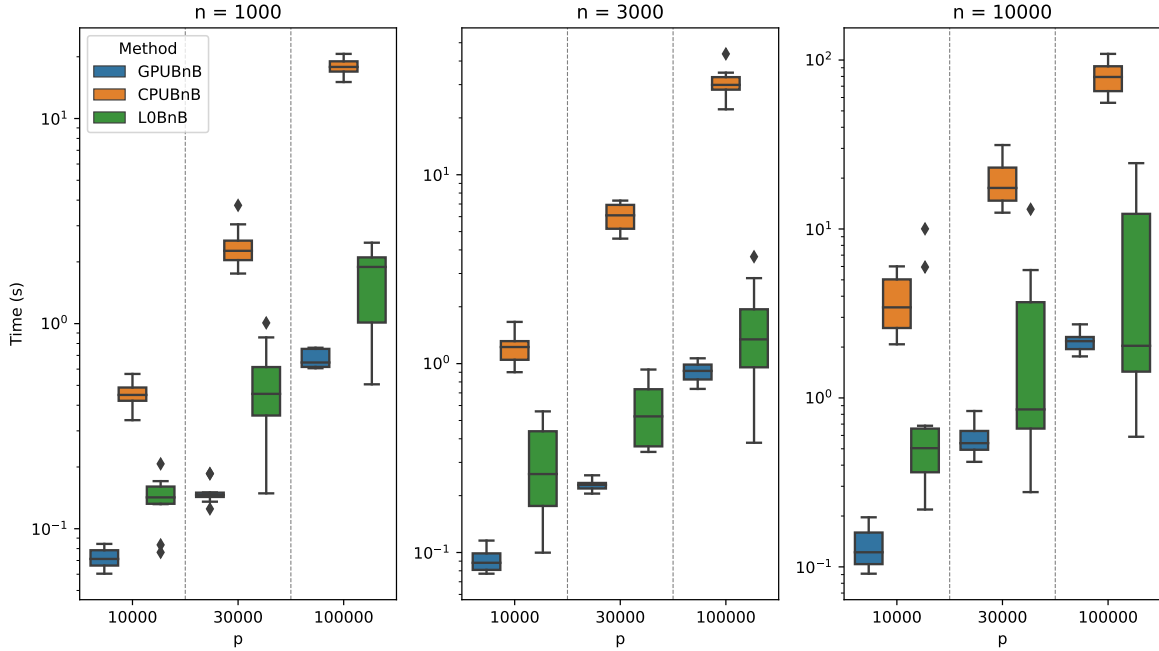


Figure 4: Average node relaxation solving time (in seconds) of our approach versus L0BnB on 10 random seeds.

- $\lambda_0 \in \{0.05, 0.2, 0.4, 0.6, 1.5, 2.0\} \cdot \lambda_0^*$

where λ_2^* and λ_0^* are optimal parameter values, as defined in Section 4.1.

SNR	GPUBnB	CPUBnB	L0BnB	k^0	GPUBnB	CPUBnB	L0BnB
0.5	(100362)	(7258)	(1846)	5	19.2	492	1.38
1	217	4992	(1777)	10	102	2461	233
2	59.1	1983	567	15	364	8669	3017
3	56.8	1884	175	20	1481	(5578)	(9597)

Table 2: Runtime (in seconds) for synthetic datasets with $n = 3000$ samples and $p = 30000$ features, varying SNR (**left**) and number of nonzeros in the true coefficient β^\dagger (**right**). If an algorithm cannot achieve 10^{-2} optimality gap within 4 hours, the number of nodes solved in 4 hours is displayed in brackets.

Tables 2 and 3 compare L0BnB with our approach across these settings (excluding MOSEK due to memory constraints). For relatively easy-to-solve problems (low noise with $\text{SNR} \geq 3$ or small k^0), L0BnB demonstrates superior performance. However, our approach performs better for harder instances (high noise or large k^0), with CPUBnB achieving up to 10x speedup over L0BnB. Similar patterns emerge with regularization parameters: L0BnB excels with larger λ_2 or λ_0 but slows down for smaller ones, while CPUBnB maintains stable performance and outperforms L0BnB for smaller λ_2 and λ_0 values.

Our GPU implementation (GPUBnB) consistently achieves 20-30x speedup over CPUBnB across all parameter settings. To further analyze GPU acceleration benefits, we evaluate our approach on various computing platforms (with specifications displayed in Table 4). Figure 5 compares the number of nodes processed within one hour across platforms, tested on synthetic datasets with

λ_2	GPUBnB	CPUBnB	L0BnB	λ_0	GPUBnB	CPUBnB	L0BnB	$\ \beta\ _0$
$0.1\lambda_2^*$	84.8	1947	470	$0.05\lambda_0^*$	(40913)	(1737)	(441)	16
$0.3\lambda_2^*$	78.1	2077	329	$0.2\lambda_0^*$	1648	(4365)	(1521)	10
$3\lambda_2^*$	24.4	608	3.43	$0.4\lambda_0^*$	7.80	275	37.2	10
$10\lambda_2^*$	9.55	370	1.12	$0.6\lambda_0^*$	12.3	440	26.2	10
$30\lambda_2^*$	2.03	76.7	1.01	$2\lambda_0^*$	243	6399	21.1	7

Table 3: Runtime (in seconds) for synthetic datasets with $n = 3000$ samples and $p = 30000$ features, varying λ_2 (**left**) and λ_0 (**right**). For varying λ_0 , we also report the number of nonzeros in the solution β obtained by each BnB method. If an algorithm cannot achieve 10^{-2} optimality gap within 4 hours, the number of nodes solved in 4 hours is displayed in brackets.

platform	processor	theoretical peak (FP64)	bandwidth
CPU	AMD EPYC 9474F 3.60GHz	66 GFLOPs	460.8GB/s
V100	NVIDIA V100-PCIe-32GB	7.1 TFLOPs	0.9TB/s
A100	NVIDIA A100-PCIe-80GB	9.7 TFLOPs	1.9TB/s
L40S	NVIDIA L40S-PCIe-48GB	1.4 TFLOPs	0.9TB/s
H100	NVIDIA H100-PCIe-80GB	25.6 TFLOPs	2TB/s

Table 4: Specifications of the computing platforms used.

$n = 3000$, $p \in \{10^4, 3 \cdot 10^4, 10^5\}$ and $\text{SNR} = 0.1$, using 10 random seeds.

The results demonstrate that GPU acceleration effectiveness varies with problem size and GPU platform. Across all test cases, our GPU implementation processes 10-40x more nodes than its CPU counterpart, highlighting the substantial benefits of GPU acceleration.

4.3 Real-world dataset

We evaluate GPUBnB and CPUBnB on the UJIIndoorLoc dataset ($n = 11,962$ samples, $p = 23,250$ features). We generate solutions with varying sparsity levels by adjusting λ_0 as multiples of λ_0^* . Figures 6 display the best optimality gaps achieved within 4 hours and the average node-solving times, respectively. On this dataset, GPUBnB processes each node approximately 30 times faster than its CPU counterpart, enabling it to achieve significantly smaller optimality gaps within the 4-hour time limit.

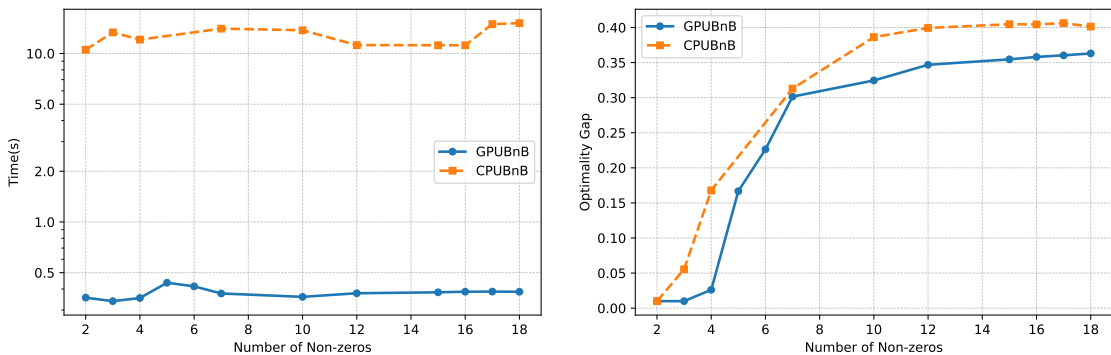


Figure 6: Performance comparison on UJIIndoorLoc dataset: (**left**) average node solving time in seconds, and (**right**) best optimality gap achieved within 4 hours, for GPU and CPU implementations of our approach.

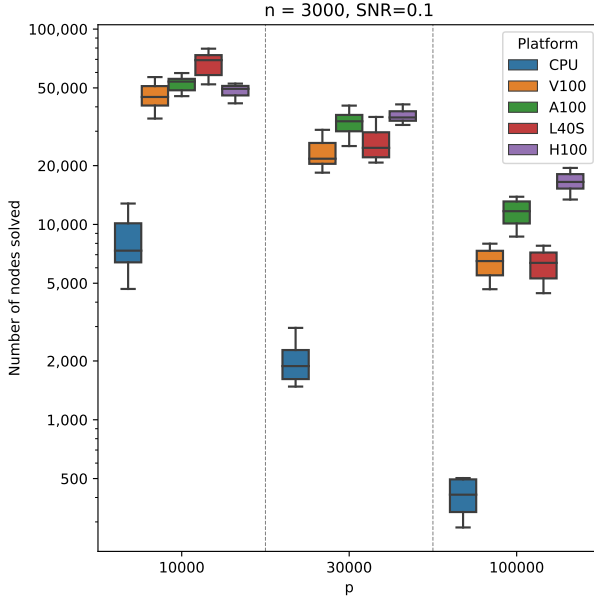


Figure 5: Number of nodes solved within one hour with CPUBnB/GPUBnB (without node parallelism) across different computing platforms. Results are shown for 10 random seeds on synthetic datasets with $n = 3000$ samples, $p = 30000$ features, and $\text{SNR} = 0.1$.

4.4 Node parallelism

As outlined in subsection 3.2, we leverage GPU parallelization by solving multiple branch-and-bound nodes simultaneously. To quantify the benefits of this approach, we conducted experiments varying the batch size K —defined as the number of nodes processed in parallel during the lower-bound evaluation step.

Experimental Design. We maintain the same data generation protocol described in Section 4.1 to ensure consistency; specifically, we utilize the same synthetic setup with $n = 3000$, $\rho = 0.2$, $k^0 = 10$, and fix the algorithm to GPUBnB. However, unlike the previous experiments where the parallelization strategy was fixed to sequential ($K = 1$), we now explicitly vary the batch size K —the number of nodes processed simultaneously by the GPU. We test varying the feature dimensions $p \in \{10^4, 3 \times 10^4, 10^5\}$. We test a range of batch sizes $K \in \{1, 10, 50, 100\}$. Note that $K = 1$ corresponds to a standard strategy without node parallelism, while e.g. $K = 50$ represents a strategy of processing 50 nodes in parallel at each step. All experiments were conducted with a fixed time limit of 3600 seconds. For $p \in \{10^4, 3 \times 10^4\}$, we run the experiments on an A100 GPU and for $p = 10^5$ we conduct the experiment on a H100 GPU.

Results. Figure 7 demonstrates the impact of different batch sizes on GPUBnB performance for the synthetic instances. The top plot illustrates the MIP optimality gap reduction over time, while the bottom plot tracks the cumulative number of nodes processed. We observe that increasing the batch size yields a significant improvement in node throughput. For the largest problem setting $p = 10^5$, using a batch size of $K = 100$ allows the algorithm to process over 25x as many nodes per second compared to the sequential baseline.

This throughput advantage translates directly to convergence speed. Larger batch sizes reduce the optimality gap down much faster in the early stages of the search. While larger batches can theoretically introduce some search overhead (processing nodes that might have been pruned given updated bounds from a sequential search), the speedup provided by saturating the GPU cores

greatly outweighs this inefficiency. Crucially, this dramatic increase in throughput does not lead to a proportional increase in GPU memory consumption. For example, at $p = 3 \times 10^4$, increasing the batch size from $K = 1$ to $K = 100$ results in a 32% increase in peak memory, despite a massive gain in processing speed. This efficiency is achieved through our shared memory reference scheme described in section 3.6: the large invariant data structures are stored once and shared across all K parallel subproblems. The only memory scaling linearly with K is the storage of the relatively small vectors of decision variables, allowing us to saturate GPU cores without exhausting memory.

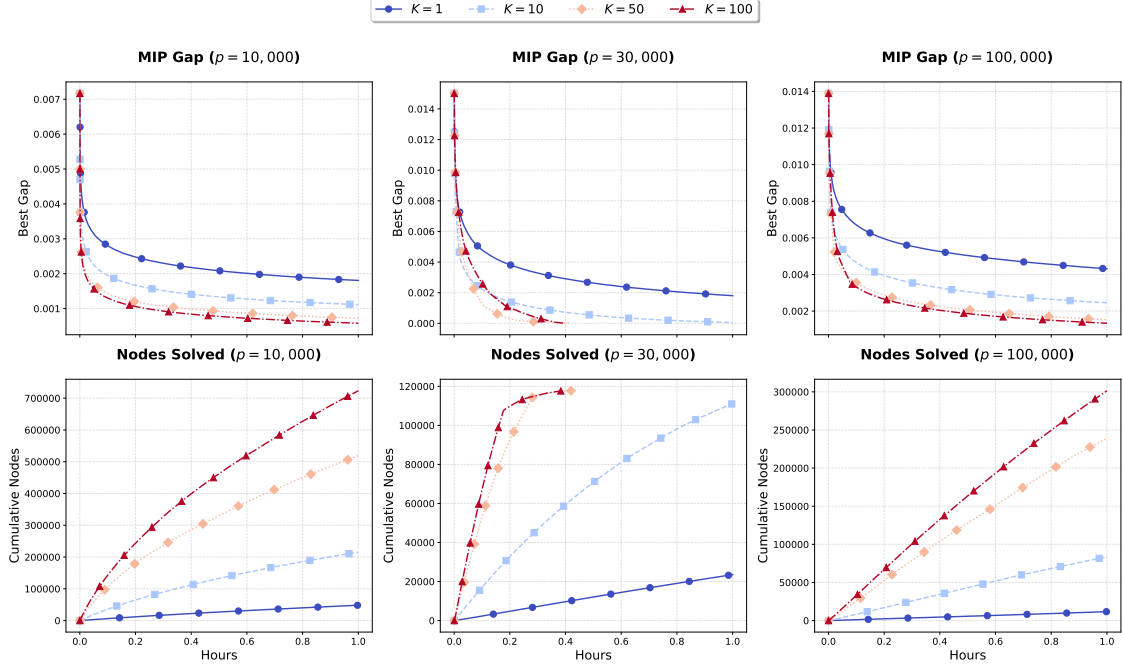


Figure 7: Synthetic examples: MIP gap (top) and number of nodes processed (bottom) with different batch sizes.

Batch (K)	$p = 10^4$		$p = 3 \times 10^4$		$p = 10^5$	
	Mem (GB)	Rel. Inc.	Mem (GB)	Rel. Inc.	Mem (GB)	Rel. Inc.
1	0.636	1.00x	1.285	1.00x	2.824	1.00x
10	0.652	1.03x	1.310	1.02x	2.983	1.06x
50	0.726	1.14x	1.459	1.14x	3.693	1.31x
100	0.816	1.28x	1.696	1.32x	4.580	1.62x

Table 5: Peak memory usage (GB) and relative increase in peak memory compared to the $K = 1$ baseline as p varies.

Acknowledgment

The authors acknowledge research support funding from the Office of Naval Research.

References

- [1] Ahmed Abbas and Paul Swoboda. Fastdog: Fast discrete optimization on gpu. In *Proceedings of the IEEE/CVF Conference on Computer Vision and Pattern Recognition (CVPR)*, pages 439–449, June 2022.
- [2] M Selim Aktürk, Alper Atamtürk, and Sinan Gürel. A strong conic quadratic reformulation for machine-job assignment with controllable processing times. *Operations Research Letters*, 37(3):187–191, 2009.
- [3] Hartwig Anzt, William Sawyer, Stanimire Tomov, Piotr Luszczek, Ichitaro Yamazaki, and Jack Dongarra. Optimizing krylov subspace solvers on graphics processing units. In *2014 IEEE International Parallel & Distributed Processing Symposium Workshops*, pages 941–949. IEEE, 2014.
- [4] MOSEK ApS. *The MOSEK optimization toolbox for Python manual. Version 9.3.*, 2022.
- [5] Alper Atamturk and Andres Gomez. Rank-one convexification for sparse regression, 2020.
- [6] Kayhan Behdin, Wenyu Chen, and Rahul Mazumder. Sparse gaussian graphical models with discrete optimization: Computational and statistical perspectives, 2023.
- [7] Kayhan Behdin and Rahul Mazumder. Sparse pca: A new scalable estimator based on integer programming, 2021.
- [8] Dimitri P Bertsekas. Nonlinear programming. *Journal of the Operational Research Society*, 48(3):334–334, 1997.
- [9] Dimitris Bertsimas and Jack Dunn. Optimal classification trees. *Machine Learning*, 106:1039–1082, 2017.
- [10] Dimitris Bertsimas and Jack Dunn. *Machine Learning under a Modern Optimization Lens*. Dynamic Ideas LLC, 2019.
- [11] Dimitris Bertsimas, Angela King, and Rahul Mazumder. Best subset selection via a modern optimization lens. *The annals of statistics*, 44(2):813–852, 2016.
- [12] Dimitris Bertsimas and Bart Van Parys. Sparse high-dimensional regression: Exact scalable algorithms and phase transitions. *The Annals of Statistics*, 48(1):300–323, 2020.
- [13] Aaresh Bhathena, Salar Fattahi, Andrés Gómez, and Simge Küçükyavuz. A parametric approach for solving convex quadratic optimization with indicators over trees, 2024.
- [14] Stephen Boyd, Neal Parikh, Eric Chu, Borja Peleato, and Jonathan Eckstein. 2011.
- [15] Ebubekir Buber and Banu Diri. Performance analysis and cpu vs gpu comparison for deep learning. pages 1–6, 2018.
- [16] Emmanuel J Candes and Mark A Davenport. How well can we estimate a sparse vector? *Applied and Computational Harmonic Analysis*, 34(2):317–323, 2013.
- [17] Jens Clausen. *Parallel Branch and Bound — Principles and Personal Experiences*, pages 239–267. Springer US, Boston, MA, 1997.

- [18] Damek Davis and Wotao Yin. Convergence rate analysis of several splitting schemes. *Splitting methods in communication, imaging, science, and engineering*, pages 115–163, 2016.
- [19] Antoine Dedieu, Hussein Hazimeh, and Rahul Mazumder. Learning sparse classifiers: Continuous and mixed integer optimization perspectives. *The Journal of Machine Learning Research*, 22(1):6008–6054, 2021.
- [20] Alyson K Fletcher, Sundeep Rangan, and Vivek K Goyal. Necessary and sufficient conditions for sparsity pattern recovery. *IEEE Transactions on Information Theory*, 55(12):5758–5772, 2009.
- [21] Anders Forsgren. On warm starts for interior methods. volume 199, pages 51–66, 07 2005.
- [22] Robert M. Freund, Paul Grigas, and Rahul Mazumder. A new perspective on boosting in linear regression via subgradient optimization and relatives, 2015.
- [23] Jerome Friedman, Trevor Hastie, and Rob Tibshirani. Regularization paths for generalized linear models via coordinate descent. *Journal of statistical software*, 33(1):1, 2010.
- [24] David Gamarnik and Ilias Zadik. High dimensional regression with binary coefficients. estimating squared error and a phase transition. In *Conference on learning theory*, pages 948–953. PMLR, 2017.
- [25] David Gamarnik and Ilias Zadik. Sparse high-dimensional linear regression. Estimating squared error and a phase transition. *The Annals of Statistics*, 50(2):880 – 903, 2022.
- [26] Bernard Gendron and Teodor Gabriel Crainic. Parallel branch-and-bound algorithms: Survey and synthesis. *Operations Research*, 42(6):1042–1066, 1994.
- [27] Eitan Greenshtein. Best subset selection, persistence in high-dimensional statistical learning and optimization under l_1 constraint. *The Annals of Statistics*, pages 2367–2386, 2006.
- [28] Andrés Gómez and José Neto. Outlier detection in regression: conic quadratic formulations, 2023.
- [29] William W. Hager. Updating the inverse of a matrix. *SIAM Review*, 31(2):221–239, 1989.
- [30] Shaoning Han and Andrés Gómez. Compact extended formulations for low-rank functions with indicator variables. *Mathematics of Operations Research*, 50(3):1992–2016, 2025.
- [31] Hussein Hazimeh and Rahul Mazumder. Fast best subset selection: Coordinate descent and local combinatorial optimization algorithms. *Operations Research*, 68(5):1517–1537, 2020.
- [32] Hussein Hazimeh, Rahul Mazumder, and Peter Radchenko. Grouped variable selection with discrete optimization: Computational and statistical perspectives, 2021.
- [33] Hussein Hazimeh, Rahul Mazumder, and Ali Saab. Sparse regression at scale: Branch-and-bound rooted in first-order optimization. *Mathematical Programming*, pages 1–42, 2021.
- [34] Jin Hyuk Jung, Jung And, and Dianne O’leary. Implementing an interior point method for linear programs on a cpu-gpu system. *Electronic Transactions on Numerical Analysis. Volume*, 28:174–189, 01 2008.

[35] Rory Kelly. Gpu computing for atmospheric modeling. *Computing in Science & Engineering*, 12(4):26–33, 2010.

[36] Siu Kwan Lam, Antoine Pitrou, and Stanley Seibert. Numba: A llvm-based python jit compiler. In *Proceedings of the Second Workshop on the LLVM Compiler Infrastructure in HPC*, pages 1–6, 2015.

[37] Jeff T Linderoth and Martin WP Savelsbergh. A computational study of search strategies for mixed integer programming. *INFORMS Journal on Computing*, 11(2):173–187, 1999.

[38] Haihao Lu and Jinwen Yang. cupdlp.jl: A gpu implementation of restarted primal-dual hybrid gradient for linear programming in julia. 2024.

[39] Rahul Mazumder, Peter Radchenko, and Antoine Dedieu. Subset selection with shrinkage: Sparse linear modeling when the snr is low, 2022.

[40] Rahul Mazumder, Peter Radchenko, and Antoine Dedieu. Subset selection with shrinkage: Sparse linear modeling when the snr is low. *Operations Research*, 2022.

[41] Sparsh Mittal and Shraiysh Vaishay. A survey of techniques for optimizing deep learning on gpus. *Journal of Systems Architecture*, 99:101635, 2019.

[42] Balas Kausik Natarajan. Sparse approximate solutions to linear systems. *SIAM journal on computing*, 24(2):227–234, 1995.

[43] Cristóbal A. Navarro, Nancy Hitschfeld-Kahler, and Luis Mateu. A survey on parallel computing and its applications in data-parallel problems using gpu architectures. *Communications in Computational Physics*, 15(2):285–329, 2014.

[44] John D. Owens, Mike Houston, David Luebke, Simon Green, John E. Stone, and James C. Phillips. Gpu computing. *Proceedings of the IEEE*, 96(5):879–899, 2008.

[45] François Pacaud, Sungho Shin, Michel Schanen, Daniel Maldonado, and Mihai Anitescu. Accelerating condensed interior-point methods on simd/gpu architectures. *Journal of Optimization Theory and Applications*, 202:1–20, 02 2023.

[46] Mohit Pandey, Michael Fernandez, Francesco Gentile, Olexandr Isayev, Alexander Tropsha, Abraham C Stern, and Artem Cherkasov. The transformational role of gpu computing and deep learning in drug discovery. *Nature Machine Intelligence*, 4(3):211–221, 2022.

[47] Adam Paszke, Sam Gross, Soumith Chintala, Gregory Chanan, Edward Yang, Zachary DeVito, Zeming Lin, Alban Desmaison, Luca Antiga, and Adam Lerer. Automatic differentiation in pytorch. 2017.

[48] Garvesh Raskutti, Martin J Wainwright, and Bin Yu. Minimax rates of estimation for high-dimensional linear regression over ℓ_q -balls. *IEEE transactions on information theory*, 57(10):6976–6994, 2011.

[49] Christian Schulz, Geir Hasle, André R. Brodtkorb, and Trond R. Hagen. Gpu computing in discrete optimization. part ii: Survey focused on routing problems. *EIRO Journal on Transportation and Logistics*, 2(1):159–186, 2013.

[50] Sungho Shin, François Pacaud, and Mihai Anitescu. Accelerating optimal power flow with gpus: Simd abstraction of nonlinear programs and condensed-space interior-point methods, 2024.

- [51] Pavel Sountsov, Colin Carroll, and Matthew D. Hoffman. Running markov chain monte carlo on modern hardware and software, 2024.
- [52] Daniele G. Spampinato and Anne C. Elster. Linear optimization on modern gpus. pages 1–8, 2009.
- [53] Kasia Świrydowicz, Eric Darve, Wesley Jones, Jonathan Maack, Shaked Regev, Michael A Saunders, Stephen J Thomas, and Slaven Peleš. Linear solvers for power grid optimization problems: a review of gpu-accelerated linear solvers. *Parallel Computing*, 111:102870, 2022.
- [54] Andreas M. Tillmann, Daniel Bienstock, Andrea Lodi, and Alexandra Schwartz. Cardinality minimization, constraints, and regularization: A survey, 2022.
- [55] Stanimire Tomov, Rajib Nath, Hatem Ltaief, and Jack Dongarra. Dense linear algebra solvers for multicore with gpu accelerators. pages 1–8, 2010.
- [56] Joaqun Torres-Sospedra, Raul Montoliu, Adolfo Martnez-Us, Tomar Arnau, and Joan Avariento. UJIIndoorLoc. UCI Machine Learning Repository, 2014. DOI: <https://doi.org/10.24432/C5MS59>.
- [57] Martin J Wainwright. Information-theoretic limits on sparsity recovery in the high-dimensional and noisy setting. *IEEE transactions on information theory*, 55(12):5728–5741, 2009.
- [58] Martin J. Wainwright. *High-Dimensional Statistics: A Non-Asymptotic Viewpoint*. Cambridge Series in Statistical and Probabilistic Mathematics. Cambridge University Press, Cambridge, 2019.
- [59] Weijun Xie and Xinwei Deng. Scalable algorithms for the sparse ridge regression. *SIAM Journal on Optimization*, 30(4):3359–3386, 2020.
- [60] Yuchen Zhang, Martin J. Wainwright, and Michael I. Jordan. Lower bounds on the performance of polynomial-time algorithms for sparse linear regression, 2014.
- [61] Yuchen Zhang, Martin J Wainwright, and Michael I Jordan. Lower bounds on the performance of polynomial-time algorithms for sparse linear regression. In *Conference on Learning Theory*, pages 921–948. PMLR, 2014.

A Additional Technical Details

A.1 Derivation of problem (4)

We simplify problem (3) by analytically solving for the optimal values of variables z and s for any fixed, feasible β , and then substituting these optimal solutions back into the original problem. This reduction allows us to reformulate the problem solely in terms of β .

Consider any feasible solution (β, z, s) to problem (3), it follows $|\beta_i| \leq Mz_i \leq M, \forall i \in [p]$. The minimization with respect to z and s can be decomposed into p independent subproblems, one for each coordinate $i \in [p]$. Specifically, for each $i \in [p]$, we solve:

$$\begin{aligned}
 \min_{z_i, s_i} \quad & \lambda_0 z_i + \lambda_2 s_i \\
 \text{s.t.} \quad & \beta_i^2 \leq s_i z_i, \quad |\beta_i| \leq M z_i, \\
 & z_i \in [0, 1], \quad s_i \geq 0, \\
 & z_i = 0 \text{ if } i \in \mathcal{F}_0, \quad z_i = 1 \text{ if } i \in \mathcal{F}_1.
 \end{aligned} \tag{29}$$

We discuss the following scenarios.

1. $i \in \mathcal{F}_0$. When $|\beta_i| \neq 0$, problem (29) is infeasible; when $\beta_i = 0$, the only feasible solution is $(z_i^*, s_i^*) = (0, 0)$, and the minimum is 0.
2. $i \in \mathcal{F}_1$. The optimal solution to problem (29) is $(z_i^*, s_i^*) = (1, \beta_i^2)$, and the minimum is $\lambda_0 + \lambda_2 \beta_i^2$.
3. $i \notin \mathcal{F}_0 \cup \mathcal{F}_1$. Note that $s_i = \beta_i^2/z_i$ is the smallest possible value s , which satisfies the constraint of problem (29) (for the case $\beta_i = z_i = 0$, define $\beta_i^2/z_i = 0$). Problem (29) then reduced to

$$\begin{aligned} \min_{z_i} \quad & \lambda_0 z_i + \lambda_2 \frac{\beta_i^2}{z_i} \\ \text{s.t.} \quad & \frac{|\beta_i|}{M} \leq z_i \leq 1. \end{aligned} \tag{30}$$

Note that the objective function $z_i \mapsto \lambda_0 z_i + \lambda_2 \frac{\beta_i^2}{z_i}$ is convex and its gradient reaches zero when $z_i = \sqrt{\frac{\lambda_2}{\lambda_0}} |\beta_i|$. We consider three cases:

- (a) $1 \leq \sqrt{\frac{\lambda_2}{\lambda_0}} |\beta_i|$. The objective is monotonically decreasing within the feasible region, therefore $(z_i^*, s_i^*) = (1, \beta_i^2/z_i^*)$ and the minimum is $\lambda_0 + \lambda_2 \beta_i^2$.
- (b) $\frac{|\beta_i|}{M} \leq \sqrt{\frac{\lambda_2}{\lambda_0}} |\beta_i| \leq 1$. By optimality condition, $(z_i^*, s_i^*) = \left(\sqrt{\frac{\lambda_2}{\lambda_0}} |\beta_i|, \beta_i^2/z_i^* \right)$ and the minimum is $2\sqrt{\lambda_0 \lambda_2} |\beta_i|$.
- (c) $\sqrt{\frac{\lambda_2}{\lambda_0}} |\beta_i| \leq \frac{|\beta_i|}{M}$. The objective is monotonically increasing within the feasible region, therefore $(z_i^*, s_i^*) = \left(\frac{|\beta_i|}{M}, \beta_i^2/z_i^* \right)$, the minimum is $\left(\frac{\lambda_0}{M} + \lambda_2 M \right) |\beta_i|$.

Summing up all the above cases, we arrive at the simplified problem (4).

Derivation of equation (12). For any given $i \in [p]$ and $\tilde{\beta}_i$, we aim to derive

$$\beta_i^* = \arg \min_{\beta_i} \frac{\rho}{2} (\beta_i - \tilde{\beta}_i)^2 + \psi_i(\beta_i; \lambda_0, \lambda_2, M) + \infty \cdot \mathbf{1}_{\{|\beta_i| \leq M\}} \tag{31}$$

We discuss the following scenarios.

1. $i \in \mathcal{F}_0$. In this case $\psi_i(\beta_i; \lambda_0, \lambda_2, M) = \infty \cdot \mathbf{1}_{\{\beta_i=0\}}$, and it is clear that $\beta_i^* = 0$.
2. $i \in \mathcal{F}_1$. In this case $\psi_i(\beta_i; \lambda_0, \lambda_2, M) = \lambda_0 + \lambda_2 \beta_i^2$, and it follows from first-order optimality conditions that

$$\beta_i^* = \text{proj}_{[-M, M]} \left(\frac{\rho}{\rho + 2\lambda_2} \tilde{\beta}_i \right) = T \left(\frac{\rho}{\rho + 2\lambda_2} \tilde{\beta}_i, 0, M \right). \tag{32}$$

3. $i \notin \mathcal{F}_0 \cup \mathcal{F}_1$ and $\sqrt{\frac{\lambda_0}{\lambda_2}} \leq M$. In this case

$$\psi_i(\beta_i; \lambda_0, \lambda_2, M) = \begin{cases} 2\sqrt{\lambda_0 \lambda_2} |\beta_i| & \text{if } |\beta_i| \leq \sqrt{\lambda_0/\lambda_2} \\ \lambda_0 + \lambda_2 \beta_i^2 & \text{else if } \sqrt{\lambda_0/\lambda_2} \leq |\beta_i| \leq M. \end{cases} \tag{33}$$

- (a) If $|\beta_i^*| \leq \sqrt{\lambda_0/\lambda_2}$, it follows from the first-order optimality conditions that β_i^* is given by the boxed version of the soft thresholding operator [23], i.e., $\beta_i^* = T \left(\tilde{\beta}_i; \frac{2\sqrt{\lambda_0 \lambda_2}}{\rho}, M \right)$. This is valid as long as $\left| T \left(\tilde{\beta}_i; \frac{2\sqrt{\lambda_0 \lambda_2}}{\rho}, M \right) \right| \leq \sqrt{\frac{\lambda_0}{\lambda_2}}$, which implies $|\tilde{\beta}_i| \leq \frac{2\sqrt{\lambda_0 \lambda_2}}{\rho} + \sqrt{\frac{\lambda_0}{\lambda_2}}$.

(b) If $|\beta_i^*| > \sqrt{\lambda_0/\lambda_2}$, similar to Case 2, $\beta_i^* = T\left(\frac{\rho}{\rho+2\lambda_2}\tilde{\beta}_i, 0, M\right)$. This is valid as long as $|T\left(\frac{\rho}{\rho+2\lambda_2}\tilde{\beta}_i, 0, M\right)| > \sqrt{\frac{\lambda_0}{\lambda_2}}$, which implies $|\tilde{\beta}_i| > \frac{2\sqrt{\lambda_0\lambda_2}}{\rho} + \sqrt{\frac{\lambda_0}{\lambda_2}}$.

4. $i \notin \mathcal{F}_0 \cup \mathcal{F}_1$ and $\sqrt{\frac{\lambda_0}{\lambda_2}} > M$. In this case $\psi_i(\beta_i; \lambda_0, \lambda_2, M) = (\lambda_0/M + \lambda_2 M)|\beta_i|$. Similar to Case 3(b), the optimal solution is given by the boxed version of the soft thresholding operator $\beta_i^* = T\left(\tilde{\beta}_i; \frac{\lambda_0}{M\rho} + \frac{\lambda_2 M}{\rho}, M\right)$.

Summing up all the above cases, we arrive at equation (12).

Proof of Theorem 1. The Lagrangian function of problem (6) is

$$L(b, \beta, v) = \frac{1}{2}\|y - Xb\|_2^2 + \sum_{i \in [p]} \psi_i(\beta_i; \lambda_0, \lambda_2, M) + \infty \cdot \mathbf{1}_{\{\|\beta\|_\infty \leq M\}} + v^\top(b - \beta) \quad (34)$$

The Lagrangian dual reads:

$$\max_{b \in \mathbb{R}^p} \min_{\beta \in \mathbb{R}^p} \frac{1}{2}\|y - Xb\|_2^2 + \sum_{i \in [p]} \psi_i(\beta_i; \lambda_0, \lambda_2, M) + \infty \cdot \mathbf{1}_{\{\|\beta\|_\infty \leq M\}} + v^\top(b - \beta) \quad (35)$$

The inner minimization problem of (35) decomposes into the following separable minimization subproblems:

$$\begin{aligned} & \min_{b, \beta} \quad \frac{1}{2}\|y - Xb\|_2^2 + \sum_{i \in [p]} \psi_i(\beta_i; \lambda_0, \lambda_2, M) + \infty \cdot \mathbf{1}_{\{\|\beta\|_\infty \leq M\}} + v^\top(b - \beta) \\ &= \min_b \frac{1}{2}\|y - Xb\|_2^2 + v^\top b + \sum_{i \in [p]} \left(\min_{\beta_i} \psi_i(\beta_i; \lambda_0, \lambda_2, M) + \infty \cdot \mathbf{1}_{\{|\beta_i| \leq M\}} - v_i \beta_i \right) \end{aligned} \quad (36)$$

If $v \notin \text{row}(X)$, there exists $b' \in \text{null}(X)$ with $v^\top b' \neq 0$. Then for any feasible solution b , the vector $b + \alpha b'$ remains feasible for all $\alpha \in \mathbb{R}$, and $v^\top(b + \alpha b')$ can be made arbitrarily small. This implies the minimization problem is unbounded below. Therefore, any dual feasible v must lie in $\text{row}(X)$, i.e., $v = X^\top r$ for some $r \in \mathbb{R}^n$. Substituting this representation into (36) yields

$$\min_b \frac{1}{2}\|y - Xb\|_2^2 + r^\top Xb + \sum_{i \in [p]} \left(\min_{\beta_i} \psi_i(\beta_i; \lambda_0, \lambda_2, M) + \infty \cdot \mathbf{1}_{\{|\beta_i| \leq M\}} - (X_i^\top r)\beta_i \right) \quad (37)$$

It follows from the first-order optimality condition that the minimizer b^* of the first subproblem satisfies $r = y - Xb^*$, and the minimum is $-\frac{1}{2}\|r\|_2^2 + y^\top r$. Next, we discuss how to solve the following problem for a given $i \in [p]$:

$$\min_{\beta_i} \psi_i(\beta_i; \lambda_0, \lambda_2, M) + \infty \cdot \mathbf{1}_{\{|\beta_i| \leq M\}} - (X_i^\top r)\beta_i \quad (38)$$

We discuss the following scenarios.

1. $i \in \mathcal{F}_0$. In this case $\psi_i(\beta_i; \lambda_0, \lambda_2, M) = \infty \cdot \mathbf{1}_{\{\beta_i=0\}}$, and it is clear that $\beta_i^* = 0$ and the minimum is 0.
2. $i \in \mathcal{F}_1$. In this case $\psi_i(\beta_i; \lambda_0, \lambda_2, M) = \lambda_0 + \lambda_2 \beta_i^2$, and it follows from first-order optimality conditions that $\beta_i^* = \text{proj}_{[-M, M]} \left(\frac{X_i^\top r}{2\lambda_2} \right)$. The minimum of (38), obtained by substituting β_i^* , is $-h(|X_i^\top r|)$. Here, $h: \mathbb{R}_{\geq 0} \rightarrow \mathbb{R}$ is defined as

$$h(x) = \begin{cases} x^2/4\lambda_2 - \lambda_0 & \text{if } x \leq 2M\lambda_2 \\ Mx - \lambda_0 - \lambda_2 M^2 & \text{otherwise.} \end{cases} \quad (39)$$

3. $i \notin \mathcal{F}_0 \cup \mathcal{F}_1$ and $\sqrt{\frac{\lambda_0}{\lambda_2}} \leq M$. In this case

$$\psi_i(\beta_i; \lambda_0, \lambda_2, M) = \begin{cases} 2\sqrt{\lambda_0\lambda_2}|\beta_i| & \text{if } |\beta_i| \leq \sqrt{\lambda_0/\lambda_2} \\ \lambda_0 + \lambda_2\beta_i^2 & \text{else if } \sqrt{\lambda_0/\lambda_2} \leq |\beta_i| \leq M. \end{cases} \quad (40)$$

For the minimizer β_i^* : if $\sqrt{\lambda_0/\lambda_2} \leq |\beta_i^*| \leq M$, then the minimum is $-h(|X_i^\top r|)$ following Case 2; if $|\beta_i^*| < \sqrt{\lambda_0/\lambda_2}$, then by first-order optimality conditions, $\beta_i^* = 0$ and the minimum is 0. Moreover, since $\sqrt{\lambda_0\lambda_2}|\beta_i| \leq \lambda_0 + \lambda_2\beta_i^2$, the minimum from Case 2 cannot exceed that from Case 3. This implies $0 \leq -h(|X_i^\top r|)$ when $|\beta_i^*| < \sqrt{\lambda_0/\lambda_2}$. Thus, the minimum can be compactly expressed as $-[h(|X_i^\top r|)]_+$.

4. $i \notin \mathcal{F}_0 \cup \mathcal{F}_1$ and $\sqrt{\frac{\lambda_0}{\lambda_2}} > M$. In this case $\psi_i(\beta_i; \lambda_0, \lambda_2, M) = (\lambda_0/M + \lambda_2M)|\beta_i|$. By the first-order optimality conditions, β_i^* can only take three values: 0, $-M$, or M . Comparing these cases, the minimum value is $-[M|X_i^\top r| - \lambda_0 - \lambda_2M^2]_+$.

Summing up all the above cases, the Lagrangian dual can be expressed as

$$\max_{r \in \mathbb{R}^n} -\frac{1}{2}\|r\|_2^2 + y^\top r - \sum_{i \in [p]} \nu_i(|X_i^\top r|) \quad (41)$$

where

$$\nu_i(x) = \begin{cases} 0 & \text{if } i \in \mathcal{F}_0 \\ h(x) & \text{else if } i \in \mathcal{F}_1 \\ [h(x)]_+ & \text{else if } \sqrt{\frac{\lambda_0}{\lambda_2}} \leq M \\ [Mx - \lambda_0 - \lambda_2M^2]_+ & \text{else if } \sqrt{\frac{\lambda_0}{\lambda_2}} > M \end{cases} \quad (42)$$

Strong duality holds for (6) since it satisfies Slater's condition [8].

A.2 Matching Pursuit Algorithm

As outlined in subsection A.2, we implement a matching pursuit-inspired algorithm at the root node, with forward and backward phases. We now explain how the algorithm works in detail. During the forward phase, we consider adding variables $j \notin S$ to the current support set S . For each candidate, we solve the optimization problem:

$$\beta_j = \arg \min_{\beta_j \in [-M, M]} \left\{ \frac{1}{2}\|r - X_j\beta_j\|_2^2 + \lambda_2\beta_j^2 + \lambda_0 \right\},$$

where $r = y - X_S\beta_S$ is the residual vector. The solution involves computing the unconstrained minimizer $\beta_j^* = \frac{c_j}{D_j}$, where $c_j = X_j^\top r$, $D_j = \|X_j\|_2^2 + 2\lambda_2$, followed by projection onto $[-M, M]$:

$$\beta_j = \text{Proj}_{[-M, M]}(\beta_j^*) = \min\{\max\{\beta_j^*, -M\}, M\}.$$

The objective change for candidate j keeping other coordinates frozen is given by:

$$\Delta_j = -\beta_j c_j + \frac{1}{2}D_j\beta_j^2 + \lambda_0.$$

Similarly, for backward selection, we fix the residuals and assess the impact of removing variables $j \in S$ by setting $\beta_j = 0$:

$$\Delta_j = \beta_j c_j + \left(\frac{1}{2}\|X_j\|_2^2 - \lambda_2 \right) \beta_j^2 - \lambda_0.$$

For both forward and backward steps, these values can be batched and calculated for all candidate variables using vectorized operations, as shown in Algorithm 3.

Algorithm 3 Parallel Matching Pursuit Algorithm

Initialize: Support set $S \leftarrow \emptyset$, coefficient vector $\beta \leftarrow \mathbf{0} \in \mathbb{R}^p$, residual $r \leftarrow y$.

Repeat

1. **Forward Selection:**

- (a) Compute $c = X_{S^c}^\top r$ and $D = \|X_{S^c}\|_2^2 + 2\lambda_2$.
- (b) Compute $\beta^* = c/D$ and project: $\beta = \text{Proj}_{[-M, M]}(\beta^*)$.
- (c) Calculate $\Delta = -\beta \odot c + 0.5\beta^2 \odot D + \lambda_0$.
- (d) Find the index $j^* = \arg \min \Delta$. If $\Delta_{j^*} < 0$, update:
 - i. $S \leftarrow S \cup \{j^*\}$.
 - ii. Update β_{j^*} and $r \leftarrow r - X_{j^*} \beta_{j^*}$.

2. **Backward Selection:**

- (a) Compute $c_S = X_S^\top r$.
- (b) Calculate $\Delta = \beta \odot c_S + (0.5\|X_S\|_2^2 - \lambda_2) \odot \beta^2 - \lambda_0$.
- (c) Find the index $j^* = \arg \min \Delta$. If $\Delta_{j^*} < 0$, update:
 - i. $S \leftarrow S \setminus \{j^*\}$.
 - ii. Update $r \leftarrow r + X_{j^*} \beta_{j^*}$, and set $\beta_{j^*} = 0$.

Until No changes in S .

Output: Support set S , coefficient vector β .
